# Exceeding equilibrium limitations: Enhanced temperature control for sustainable decentralized green ammonia production − a techno-economic analysis

Asgharian, Hossein; Pignataro, Valeria ; Iov, Florin; Nielsen, Mads Pagh; Liso, Vincenzo

*Published in:*
Energy Conversion and Management

*DOI (link to publication from Publisher):*
10.1016/j.enconman.2024.118764



*Publication date:*
2024

*Document Version*
Publisher's PDF, also known as Version of record

Energy Conversion and Management 315 (2024) 118764

Contents lists available at ScienceDirect

Energy Conversion and Management

journal homepage: www.elsevier.com/locate/enconman

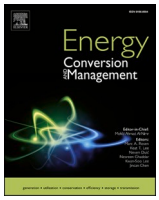

Research Paper

# Exceeding equilibrium limitations: Enhanced temperature control for sustainable decentralized green ammonia production – a techno-economic analysis

Hossein Asgharian [a,*], Valeria Pignataro [b], Florin Iov [a], Mads Pagh Nielsen [a], Vincenzo Liso [a]

[a] Department of AAU Energy, Aalborg University, Pontoppidanstræde 111, 9220 Aalborg, Denmark
[b] University of Pisa, Department of Energy, Systems, Territory and Construction Engineering, Pisa, Italy

ARTICLE INFO

*Keywords:*
Green ammonia production
Alkaline electrolyser
Modelling
Green hydrogen production

ABSTRACT

The focus on green ammonia production has intensified due to its reduced power consumption, independence from fossil fuels, and elimination of carbon dioxide ($CO_2$) emissions. Unlike conventional Haber-Bosch processes, which rely on hydrogen produced by fossil fuels and chillers to separate ammonia from unreacted gases and are constrained by equilibrium limitations, green ammonia production methods utilize hydrogen generated by water electrolysis. They typically employ metal halide materials for ammonia separation, enabling them to surpass equilibrium constraints. This study proposes a novel configuration for synthesis of green ammonia at elevated temperatures and facilitating its absorption at lower temperatures. Furthermore, it presents a comprehensive model of an alkaline electrolyser to supply the required hydrogen for green ammonia production. Additionally, this study proposes a novel method for cooling the electrolyte, leading to a 13.27% enhancement in the electrolysers system efficiency. Moreover, the analysis indicates that the proposed green ammonia production approach could reduce the power consumption by 46.2% compared to the green Haber-Bosch process. The economic analysis indicates that the proposed cooling method can reduce ammonia production costs by up to 19%, based on the electricity prices in 2023.

## 1. Introduction

Ammonia is widely regarded as a highly significant chemical product with numerous applications [1–3]. Notably, it can be utilized as an efficient and cost-effective refrigerant that poses no harm to the environment. Moreover, it has the capability to entirely substitute chlorofluorocarbons (CFCs) and hydrochlorofluorocarbons (HCFCs) in refrigeration systems [4]. Moreover, ammonia finds extensive application in the pharmaceutical industry for the production of active pharmaceutical ingredients (APIs) [5]. Ammonia also serves as a fundamental raw material to produce a wide range of nitrogen-based fertilizers [6]. In this context, it is important to emphasize that a significant portion, ranging from 75 to 90 % of the ammonia produced worldwide is dedicated to fertilizer production. Moreover, approximately 50 % of the global food production industries rely on fertilizers derived from ammonia [7]. Ammonia has also been recognized as a promising carbon-free fuel with high hydrogen density, particularly for maritime applications [8]. Indeed, it is worth noting that ammonia not only proves to be more cost-effective and possesses a higher energy density than hydrogen but also benefits from an already established infrastructure for production and distribution [9]. However, despite all the advantages of using ammonia as fuel, there are several challenges when using ammonia in combustion engines for power generation. In other words, when utilizing pure ammonia in combustion engines, achieving a high compression ratio and elevated boost pressure is crucial to overcome the slow flame speed and ensure effective combustion of ammonia [10]. The utilization of ammonia as a marine fuel offers specific advantages, particularly due to the possibility of installing complementary after treatment systems to mitigate the nitrogen oxides derivatives ($NO_x$) emissions and enhance ammonia combustion efficiency. Using ammonia as dual fuel for ships has demonstrated a reduction of greenhouse gas emissions by 34.5 % per ton-km [11].

Nitrogen ($N_2$) and hydrogen ($H_2$) serve as reactants in the production of ammonia. The necessary hydrogen can be produced from fossil fuels, with the most widely used method being steam methane reforming (SMR). In addition to hydrogen production from fossil fuels, alternative

* Corresponding author.
*E-mail address:* hoas@energy.aau.dk (H. Asgharian).

https://doi.org/10.1016/j.enconman.2024.118764
Received 29 April 2024; Received in revised form 10 June 2024; Accepted 1 July 2024
Available online 4 July 2024

methods such as microbial hydrogen production, biomass-based hydrogen production, water electrolysis and thermolysis, as well as thermochemical cycles, can also be employed [12]. Utilizing SMR for hydrogen production not only depletes fossil fuel reservoirs but also emits substantial amounts of $CO_2$. In other words, producing 1 kg of hydrogen using SMR results in emitting 8.9 kg of $CO_2$ [13]. Hence, water electrolysis is gaining more popularity for large-scale hydrogen production. Alkaline electrolysis (AEL), proton-exchange membrane (PEMEL), and solid oxide electrolysis (SOEL) are the most popular technologies for water electrolysis. Vida et al. [14] compared the performance of AEL, SOEL, and PEMEL. Their analysis revealed that AEL exhibits the longest lifetime, reaching up to 120,000 h, coupled with the lowest degradation rate ranging from 0.25 % to 1.5 % per year. Additionally, AEL boasts the lowest capital cost, falling within the range of €740 to €1,390 per kilowatt-hour (kWh). Additionally, their research demonstrated that the efficiency of AEL varies in the range of 51–60 %, surpassing that of PEMEL but falling short of SOEL. Li et al. [15] showed that when coupled with wind turbines and operating during off-grid hours, a 4 kW AEL stack can generate 1.374 million tons of hydrogen annually. Firdous et al. [16] conducted a comprehensive evaluation of power-to-hydrogen systems, particularly in their integration with hydrogen-consuming industries, utilizing renewable-rich power systems to operate hydrogen electrolysers. They developed an accurate PEMEL model, considering fluctuating current, nonlinear efficiency, system loading, and energy demands within extensive renewable energy scenarios. The study demonstrates that the model precisely estimates total operational costs, leading to improved economic outcomes and optimized utilization of renewable energy sources. Wang et al. [17] also assessed a 5 kW hybrid system consisting of a SOEL and a solar steam generator. The study revealed that the efficiency of hydrogen production in the hybrid system can attain 95.2 % under conditions where solar irradiation power reaches 2.26 kW and the SOEL operates at 700 °C. Mazza et al. [18] carried out a feasibility study on green hydrogen production using electrolysers at three locations in Tunisia. They integrated local weather data and the technical characteristics of the employed technologies into their models. The study revealed that the levelized cost of hydrogen production varies from1.34 $\$/kg_{H_2}$ and 4.06 $\$/kg_{H_2}$ depending on the location, the renewable energy sources used, and the type of electrolysers. Sanchez et al. [19] introduced a semi-empirical model for assessing the operational characteristics of a 15 kW AEL. They validated their model using experimental data, revealing that the average prediction error for cell voltage remains below 5.67 mV. Additionally, this model reliably predicts Faraday efficiency and the diffusion of hydrogen to oxygen (HTO) with errors below 1 %.

Currently, the Haber-Bosch process stands as the most prevalent method for ammonia production, satisfying over 96 % of the global demand [20]. However, this approach heavily relies on fossil fuels for hydrogen production. It operates at elevated pressures ranging from 100 to 250 bar, with 15–20 % ammonia conversion [21]. Consequently, it becomes imperative to condense the produced ammonia, separate it from the reactants, and recycle the unreacted gases back into the reactor. This method demands significant energy input, not only for the ammonia condensation process, which requires temperatures as low as −20 °C to achieve a purity of 99.6 % [22], but also for compressing the reactants to such high pressures. Additionally, the utilization of fossil fuels for hydrogen generation, coupled with the substantial energy demands of ammonia production via the Haber-Bosch process, contributes significantly to elevated $CO_2$ emissions. To address this issue, Cameli et al. [23] proposed green ammonia production via the Haber-Bosch process. In this scenario, instead of hydrogen production through SMR, PEMELs were utilized to supply the necessary hydrogen, while the required nitrogen was obtained from a cryogenic air separation unit (CASU). This study indicates that substituting the traditional Haber-Bosch process with the presented green Haber-Bosch process, employing this electrified method, can reduce $CO_2$ emissions from 1.6 $kg_{CO_2}/kg_{NH_3}$ to 0.33 $kg_{CO_2}/kg_{NH_3}$. Nowicki et al. [24] also assessed green ammonia production via the Haber-Bosch process. In their study, SOEL were employed for hydrogen production, while the necessary nitrogen was extracted from air utilizing a series of solid electrolyte oxygen pumps. The study indicated that the specific energy requirement for ammonia production using this method is 9.94 $kWh/kg_{NH_3}$. Lin et al. [25] also assessed the process of green ammonia production using SOEL, CASU, and the Haber-Bosch process. In their study, they utilized SOEL powered by solar energy for hydrogen production. They employed a novel parabolic dish equipped with wavelength-selective filter-coated photovoltaics to convert solar energy into heat and electricity, enabling the operation of the SOEL.

The utilization of sorbent material for ammonia absorption and separation has been studied by Palys et al. [26]. In their study, they used $MgCl_2$ as the sorbent material and developed kinetics for ammonia absorption and desorption. They indicated that the partial pressure of ammonia has a significant impact on the rate of ammonia absorption and desorption. The utilization of $MgCl_2$ for ammonia absorption and separation, which is crucial for exceeding the equilibrium limitation, was also studied by Onuoha et al. [27]. In their study, they highlighted that the regeneration temperature and partial pressure of ammonia, largely influenced by the sweep flow and desorption pressure, are the two driving forces for the regeneration of sorbent material. They demonstrated that the sorbent material can be regenerated at 200 °C using an exceedingly low sweep flow, resulting in ammonia release with 72 mol% purity. Smith et al. [28] also evaluated surpassing the single-pass equilibrium in ammonia production using a 5 %Ru/10 %Cs/CeO2 catalyst. In this study, they indicated that exceeding the equilibrium limit was achievable through the use of multiple catalyst and absorption layers. They demonstrated that employing a single catalyst layer operating at 363 °C resulted in a fractional conversion of 14.4 %. However, by employing three catalyst layers and two absorption layers between them, the fractional conversion increased to 24.9 %, surpassing the equilibrium limit of 21 %.

Therefore, this study proposes a more energy-efficient method for ammonia production in the context of green ammonia production. Instead of relying on hydrogen production using fossil fuels, which entails high $CO_2$ emissions, a modular system of AEL, powered by renewable energy sources, is employed. To enhance the energy efficiency of the AEL, a novel method for cooling the electrolyte is proposed, capable of significantly reducing energy consumption and improving the system efficiency. The proposed green ammonia production method is not limited by equilibrium constraints due to ammonia absorption and separation, enabling the conversion of over 90 % of fed hydrogen into ammonia in a single pass. Consequently, this method operates at lower pressure and eliminates the need for a chiller for ammonia condensation and separation, further enhancing energy efficiency. Additionally, this study proposes a novel configuration for green ammonia production, allowing for ammonia generation at elevated temperatures while absorbing ammonia at lower temperatures to optimize catalyst and sorbent material performance. Additionally, this study considered the green Haber-Bosch process as a benchmark for green ammonia production and compared the performance of the proposed method with it, utilizing the same catalyst. This comparison aimed to emphasize the energy efficiency of the suggested configuration. This study performed an economic analysis on the proposed green ammonia production system to evaluate the cost of ammonia production. Models for evaluating the process are developed using Aspen Plus and MATLAB. In this case, the AEL is modelled in Aspen Plus. This study evaluated the transient behavior of sorbent materials during ammonia absorption and desorption by developing 1D models in MATLAB. Subsequently, the integration of sorbent material with catalyst for the ammonia production process was investigated in Aspen Plus.

## 2. Methodology

In this section, the process for green ammonia production is detailed, focusing on modeling the modular system of AEL in Aspen Plus, which provides the necessary hydrogen for green ammonia production. Additionally, this section explores the kinetic models utilized in Aspen Plus and MATLAB for the generation of green ammonia.

### 2.1. Process description

This section outlines the process flow diagram modeled in Aspen Plus and MATLAB for decentralized green ammonia production with a capacity of 66 $\frac{ton_{NH_3}}{year}$. As depicted in Fig. 1, an electrolyte containing a solution of 35 wt% potassium hydroxide (KOH) enters the module of an alkaline electrolyser comprising 20 stacks (state 1). Consequently, deionized water undergoes decomposition into hydrogen and oxygen, leading to an increase in the electrolyte's temperature. As a result, the produced hydrogen and oxygen, dissolved in the electrolyte, exit the module. The oxygen stream (state 5), containing electrolyte and trace amounts of hydrogen due to cross-over, is directed to a flash tank to separate its electrolyte content. Subsequently, the oxygen stream exits the flash tank from the top (state 9), while the separated electrolyte stream, combined with makeup water, exits from the bottom (state 6). Fig. 1 also illustrates the separation of electrolyte (state 3) from hydrogen (state 23) in a flash tank, followed by electrolyte pressurization via a pump (state 4) and mixing with pressurized electrolyte separated from the oxygen stream (state 7). Notably, due to power losses in the electrolyser module, the electrolyte heats up as water decomposes, necessitating the cooling of the electrolyte before entering the stack. Traditionally, an air-cooling system achieves this by cooling water, subsequently cooling the electrolyte. However, this study proposes an efficient cooling method, substantially reducing parasitic power consumption. Here, pressurized air (state 16) comes into direct contact with water (state 22), lowering its temperature (state 18) and thus cooling the electrolyte (state 1). This direct cooling approach offers significant advantages, not only removing the minimum temperature approach limitation in the heat exchangers, but also cooling the water through evaporation. Consequently, a substantially lower mass flow rate of pressurized air is required, resulting in significantly reduced power consumption in the blower.

The generated hydrogen (state 23) is initially water-cooled, and its water content (state 25) is subsequently separated using a flash tank (state 26). Following this, it undergoes complete drying via a desiccant dryer (state 27) and is pressurized using a compressor (state 28) to 55 bars to meet the operating conditions for ammonia synthesis. As shown in Fig. 1, this study considered a CASU for supplying the required nitrogen for ammonia synthesis. This study does not focus on optimizing the CASU and the because of that it considers a simple two-column CASU which can generate nitrogen with high purities exceeding 99.99 %. According to [29] the oxygen content of the reactants should be maintained below 10 PPM to avoid poisoning of the catalyst. Hence, the designed CASU generates a nitrogen stream which contains less than 9 PPM oxygen to assure that the reactants do not affect the catalyst adversely. As shown in Fig. 1, the inlet stream to the CASU is dried air without any pollution with composition of 20.95 mol% oxygen, 78.1 mol% nitrogen, and 0.95 mol% argon. As can be seen, a compressor elevates the air pressure to 6.5 bar (state 31). Following this, the pressurized air stream is split into two separate streams. The temperature of the primary stream is lowered to −166 °C (state 39) as it enters a multi-stream heat exchanger and exchanges heat with the cold products

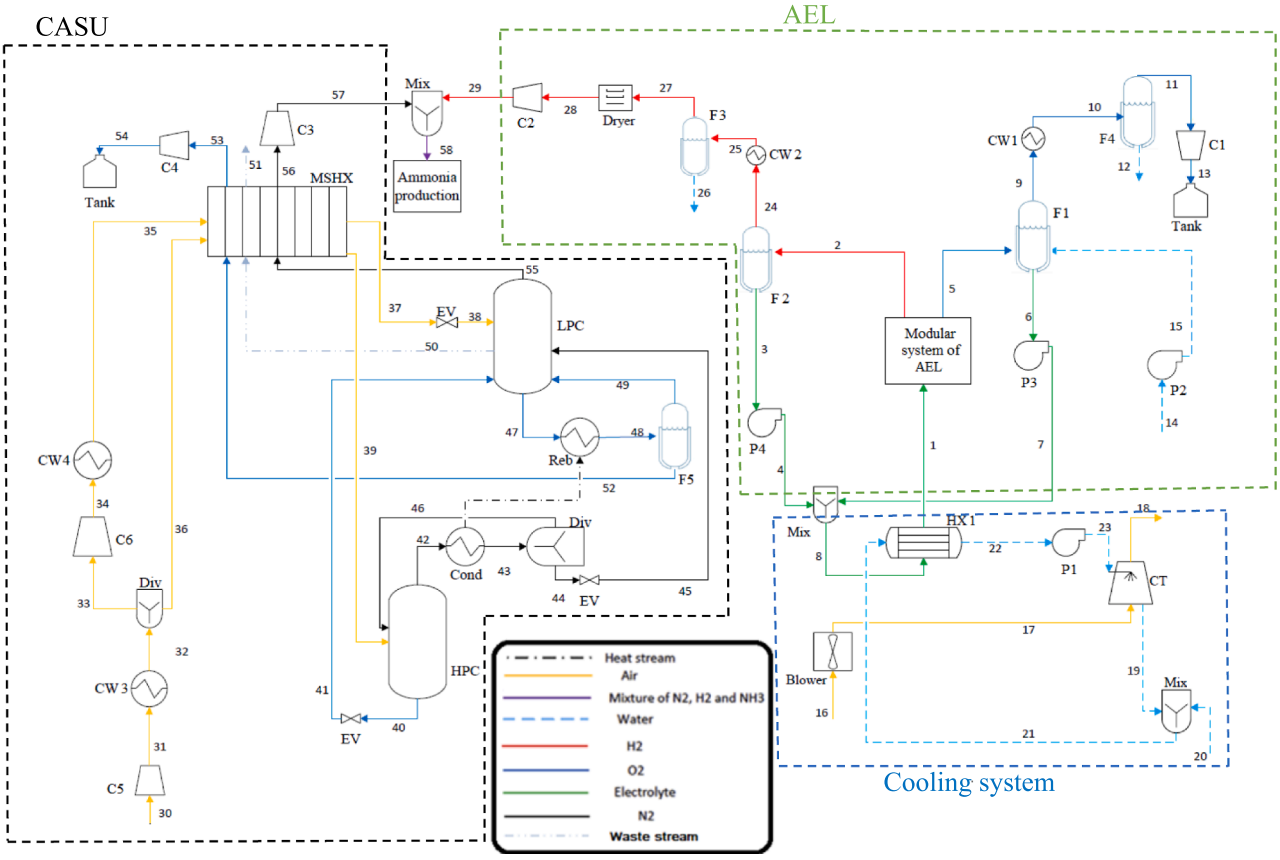


**Fig. 1.** Simplified process flow diagram of hydrogen and nitrogen production (F: Flash, CT: Cooling tower, HPC: High pressure column, LPC: Low pressure column, C: Compressor, Reb: Reboiler, Cond: Condenser, EV: Expansion valve, MSHX: Multi-stream heat exchanger, CW: Cooling water, HX: Heat exchanger, P: Pump, Mix: Mixer, Div: Divider).

exiting the CASU. Subsequently, it is directed to the high-pressure column (HPC) operating at 5 bars. The secondary stream undergoes further pressurization by the second compressor prior to its entry into the multi-stream heat exchanger. Upon cooling to −166 °C (state 37), this stream transitions into a liquid phase by exchanging heat with the cold streams. Subsequently, it undergoes expansion through an expansion valve, resulting in a temperature reduction to −191 °C (state 38), before being directed into the low-pressure column (LPC). Fig. 1 highlights the heat integration between the HPC and LPC. In this integration, the HPC condenser which condenses the rich nitrogen stream (state 43), supplies the required heat for the LPC reboiler. A portion of the rich nitrogen stream, having transitioned into the liquid phase (state 46), is recycled back to the HPC, whereas the remaining stream (state 44) undergoes expansion (state 45) before entering the LPC. The rich oxygen stream (state 40), exiting the bottom of the HPC in liquid form, undergoes expansion to 1.3 bar (state 41) before being directed to the LPC. The LPC produces nitrogen of exceedingly high purity (state 55) in its gaseous phase, which leaves the column from the top and is then directed to the multi-stream heat exchanger to be brought to ambient temperature by cooling the hot streams. The oxygen stream, with a relatively high purity exceeding 99.85 mol%, exits the flash tank from the bottom in liquid phase (state 52) and is then directed to the multi-stream heat exchanger. As depicted in Fig. 1, alongside the oxygen and nitrogen streams, a waste stream (state 50) exits the LPC, joining the multi-stream heat exchanger alongside these product streams. Consequently, the waste stream, nitrogen stream, and oxygen stream undergo heating in the multi-stream heat exchanger by exchanging heat with the incoming air streams. The produced oxygen stream is pressurized to 30 bars for storage in the vessel, while the nitrogen stream is compressed to 55 bars to meet the pressure requirements for ammonia production.

As shown in Fig. 2, the catalyst beds utilized in the ammonia production process operate in adiabatic mode, employing a 5 %Ru/10 %Cs/$CeO_2$ catalyst, with a gas hourly space velocity (GHSV) set at 20,000 $h^{-1}$ for the first catalyst bed. It is important to note that ammonia synthesis is an exothermic reaction constrained by equilibrium. Consequently, a portion of the reactants is converted to ammonia, leading to an increase in the temperature of the gas mixture at the outlet of the reactor (state 33). To overcome the equilibrium limitations and achieve the conversion of more than 90 % of the fed hydrogen into ammonia in a single pass, the synthesized ammonia in the outlet stream of the catalyst bed is separated using sorption beds containing $MgCl_2$. As a result of ammonia absorption, the concentration of generated ammonia in the gas mixture is substantially reduced, which is a key factor in achieving the conversion of more than 90 % of the fed hydrogen into ammonia in a single pass. However, the sorption beds struggle at high temperatures, necessitating the cooling of the gas mixture leaving the catalyst bed. In this setup, mineral oil (state 71) is used to cool down the outlet stream from the catalyst bed (state 61). The cooled gas mixture (state 62) then enters the sorption bed for absorption and removal of the ammonia content in the gas mixture. Three sorption beds are employed to absorb ammonia generated in each catalyst bed. In this arrangement, one bed absorbs ammonia while another bed is regenerated by receiving heat from the third sorption bed, which is being cooled. After separation of ammonia absorbed in the sorption bed, the gas mixture, primarily composed of nitrogen and hydrogen (state 63), is heated (state 64) by cooling the hot mineral oil (state 72) before entering the second reactor. It is worth noting that the mass flow rate of the gas after each sorption layer decreases due to the absorption and separation of the synthesized ammonia. Consequently, the mass flow rate of the mineral oil, which heats and cools the gas mixture, should also decrease. Thus, a portion of the mineral oil stream (state 79) is separated from the mainstream (state 75) before cooling down the gas mixture at the outlet of the reactor. Although 15 catalyst layers, each integrated with three sorption beds, are required to convert more than 90 % of the fed hydrogen into ammonia, for simplicity, only two of them are shown in Fig. 2. After achieving the desired conversion, the unreacted gases, containing traces of ammonia, are pressurized (state 68) and recycled to mix with the fresh stream of reactants (state 59) for ammonia synthesis. As mentioned above, the use of 15 catalyst layers, each integrated with three sorption beds, allows for exceeding the equilibrium limitations and achieving the conversion of over 90 % of the fed hydrogen into ammonia in a single pass. In this configuration, after each ammonia synthesis reactor, the mole fraction of ammonia is substantially reduced due to ammonia absorption and separation within the sorption beds. This reduction allows the gas mixture, now depleted of ammonia and enriched with high concentrations of reactants, to be effectively converted into ammonia in the subsequent catalyst layer. However, in this design, the gas mixture needs to pass through 15 layers of catalyst and sorbent material to achieve the desired conversion. In other words, the process of ammonia synthesis and separation through absorption needs to be repeated across these 15 layers of catalyst and sorbent material, respectively, in order to convert more than 90 % of fed hydrogen into ammonia.

Table 1 summarizes the primary characteristics of the components depicted in Fig. 1and 2. As will be discussed later, ammonia productivity

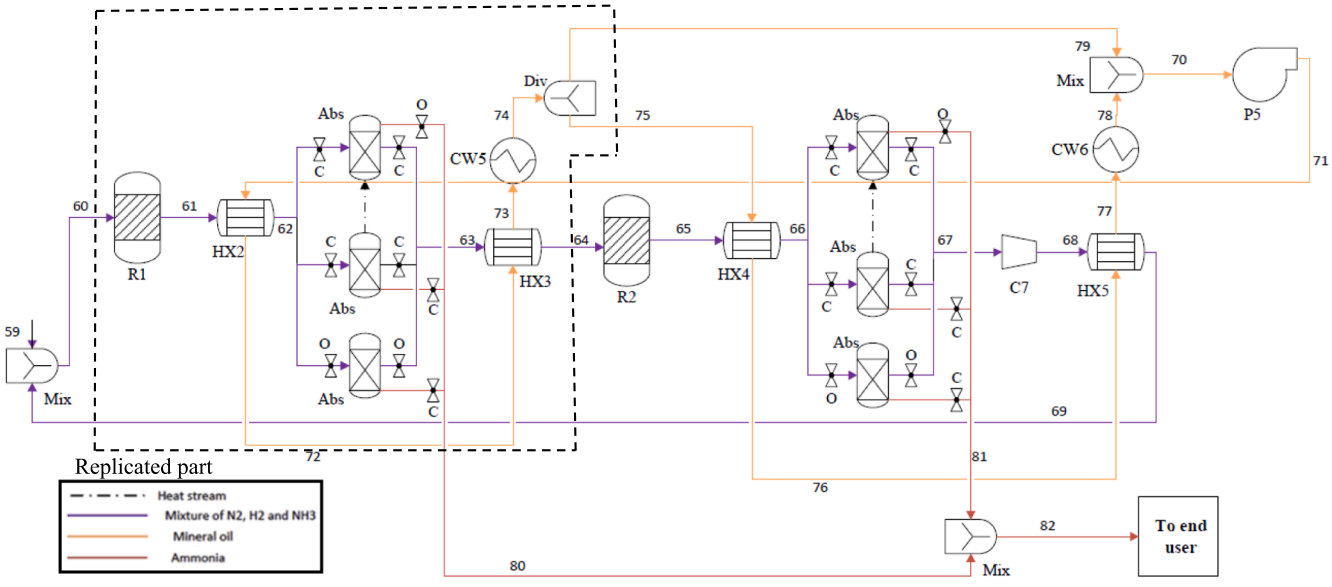


**Fig. 2.** Simplified process flow diagram of green ammonia production (Abs: Absorption layer, R: Reactor, O: Open, C: Closed).

**Table 1**
The main characteristics of the green ammonia production process shown by Figs. 1 and 2.

| | |
|---|---|
| Number of stacks with the modular system | 20 |
| Number of stack cells | 12 |
| Nominal hydrogen production capacity (kmol/hr) | 0.76 |
| Minimum temperature approach in the heat exchangers (°C) | 2 |
| Pressure drops in the heat exchangers (bar) | 0.3 |
| Isentropic efficiency of the blower and compressors | 0.7 |
| The length of the catalyst bed (m) | 0.4954 |
| Diameter of the catalyst bed (m) | 0.06 |
| Diameter of sorbent container (m) | 0.16 |

decreases when proceeding from the first catalyst bed to the last one. Consequently, the necessary mass of sorption material will vary for 1 h of operation, decreasing from the first to the last catalyst bed. Therefore, the dimensions of the sorbent material are not provided in Table 1, as they vary for different catalyst layers depending on the ammonia production rate.

### 2.2. Model description

This section outlines the models utilized in Aspen Plus and MATLAB to simulate the production of green ammonia using the configuration illustrated in Figs. 1 and 2. Initially, the discussion delves into the green hydrogen production via the AEL system in detail, followed by an elaboration on the ammonia production method, encompassing catalyst and sorption beds.

#### 2.2.1. Alkaline electrolyser

In this study, the operation of an AEL is modelled using Aspen Plus. A modular configuration was used for the stacks, so the water-splitting reaction takes place in 20 stacks with a nominal hydrogen production capacity of 0.79 kmol/hr. In modeling stacks, the framework proposed by Sànchez et al. [19,30] served as a reference and the proposed semi-empirical equations were employed in Aspen Plus to model the stacks. Thus, the RSTOIC reactor available in Aspen Plus was utilized, employing the ELECNRTL model to simulate the electrolyte within the Aspen Plus environment.

Each stack of the electrolysis system is powered by electricity. Electrical and thermal energy are employed to facilitate the electrochemical splitting of water into gaseous hydrogen and oxygen as follows:

$$H_2O(l) \rightarrow H_2(g) + \frac{1}{2}O_2(g) \tag{1}$$

The total energy demand for electrolysis equals the difference in enthalpy between the products and the reactants, supplied partially as thermal energy and partially as electrical energy. These two terms' magnitudes depend heavily on temperature. Notably, the minimum electrical demand decreases with rising temperature, while the heat demand increases [31]. The theoretical minimum cell voltage during electrolysis, indicated by the reversible cell voltage $U_{rev}$ (V), exhibits a direct correlation with the change in Gibbs free energy ΔG (J) [31], and can be expressed as:

$$U_{rev} = \frac{\Delta G}{zF} \tag{2}$$

where F is the Faraday constant (As/mol) and z is the number of electrons transferred in the reaction (z = 2). Nevertheless, the stack operations are influenced by irreversibilities, known as overvoltages, which result in cell heating and necessitate external cooling. The cell voltage (V) can be expressed as the sum of the reversible voltage and the overvoltages:

$$U_{cell} = U_{rev} + U_{ohm} + U_{act} + U_{conc} \tag{3}$$

where $U_{ohm}$ is the ohmic overvoltage and is associated with the electrical resistance of the stack components. It varies linearly with the current density according to Ohm's law. $U_{act}$ is the activation overvoltage and it is linked to exceeding the activation energy required for the hydrogen and oxygen formation reaction [19]. $U_{conc}$ represents limitations in mass transport, typically occurring at high currents. However, it can be disregarded at the typical current densities found in industrial alkaline electrolysers [32].

A valid parametric expression to express the cell voltage as a function of the temperature, pressure and current of the stack is given using the following equation [30]:

$$U_{cell} = U_{rev} + [r_1 + d_1 + r_2 T + d_2 P]i + s.log[\left(t_1 + \frac{t_2}{T} + \frac{t_3}{T^2}\right)i + 1] \tag{4}$$

where $r_j$ and $d_j$ (j = 1,2) and $t_k$ (k = 1,2,3), and s are constants given in reference [30], while T, P, and i denote the operating stack temperature (°C), pressure (bar), and current density ($A/m^2$), respectively. $U_{rev}$ is also the reversible voltage used in equation (4) can be expressed with the Nerst equation as follows [32]:

$$U_{rev} = U^0_{rev} + \frac{RT}{zF}\ln\left(\frac{(P - P_{v,KOH})^{1.5}}{a_{H2O,KOH}}\right) \tag{5}$$

where $U^0_{rev}$ is the standard equilibrium potential, R is the gas constant (J $K^{-1}$ $mol^{-1}$), $P_{v,KOH}$ is the pressure vapor of the solution (bar), and $a_{H2O,KOH}$ is the water activity (%) of the KOH solute.

Generally, alkaline electrolysers are suitable for stationary applications, as opposed to polymer membrane electrolysers, whose flexibility also makes them suitable for couplings with variable energy sources [31]. At low current densities, alkaline electrolysers can be adversely affected by the gas cross-over phenomenon [33] due to the absence of a membrane. For this reason, part-load operations are a critical aspect of alkaline electrolysers. Due to safety considerations, they typically have the capability to operate within a range of 20–100 % of the rated power [34].

In this context, the need for a gas purity model can be deduced, which can generally be expressed through two parameters: the diffusion of hydrogen to oxygen (HTO) and the diffusion of oxygen to hydrogen (OTH). Of the two parameters, only the first has been modeled as it is the most critical, and it can be calculated according to [30] as:

$$\begin{aligned} HTO(\%) = {} & C_1 + C_2 T + C_3 T^2 + \left(C_4 + C_5 T\right. \\ & \left. + C_6 T^2\right) exp\left(\frac{C_7 + C_8 T + C_9 T^2}{i}\right) + E_1 + E_2 P + E_3 P^2 + \left(E_4\right. \\ & \left. + E_5 P + E_6 P^2\right) \exp\left(\frac{E_7 + E_8 P + E_9 P^2}{i}\right) \end{aligned} \tag{6}$$

where $C_i$ (i = 1:9) and $E_i$ (i = 1:9) are constants given in reference [30]. According to equation (6), the HTO exhibits a strong dependence on temperature. This study did not account for the diffusion of oxygen to hydrogen (OTH) due to its negligible value, which typically fluctuates within the range of 0.1 % to 0.5 % [30]. On the other hand, HTO not only impacts the purity of the generated oxygen and the efficiency of the system, but also may lead to severe safety issues as both product gases can form explosive mixtures. Consequently, it needs to be maintained below 4 % to prevent explosions [35].

In an alkaline electrolyser, hydrogen production strongly relies on the operating current (I), the number of free electrons (z), and the Faraday constant (F). It can be calculated as a function of the electric current following Faraday's law [19]. However, due to the current losses, the actual behavior of an electrolyser deviates from the ideal one, so the hydrogen production will be lower. This discrepancy between ideal and actual production depends on the stack temperature and the current density [36], and this discrepancy between ideal and actual production

is given by the Faraday efficiency. Hence, the following empirical expression can be used to calculate this parameter [30]:

$$\eta_F = \frac{i^2}{f_{11} + f_{12}T + i^2}(f_{21} + f_{22}T) \tag{7}$$

where $f_i$ (i = 11, 12, 21, 22) is constant given in reference [30]. Once the Faraday efficiency is calculated, the total hydrogen production rate (mol/s) within the modular system of the AEL can be determined using the following equation:

$$\dot{n}_{H2} = \eta_F \frac{I}{zF} n_{cell,stack} n_{stack} \tag{8}$$

where $n_{cell,stack}$ and $n_{stack}$ represent the number of cells of each stack and the total number of stacks within the modular system of AEL, respectively.

The required power (W) for water electrolysis within the stacks which make the modular system can be calculated using the following equation:

$$P_{module} = U_{cell} n_{cell,stack} n_{stack} i A_{act} \tag{9}$$

where $A_{act}$ ($m^2$) represents the cell active area. It is worth noting that equation (9) only accounts for the power consumption in the stacks and excludes the power consumption within auxiliary components like pumps and blowers.

The efficiency of the stacks within the module can be calculated by dividing the higher heating value of the hydrogen generated by the electrolyzers by the power consumption of the stacks that comprise the module, as follows: [31]:

$$\eta_{module} = \frac{\dot{V}_{H_2} \bullet HHV_{H2}}{P_{module}} \tag{10}$$

However, a real system demands additional energy due to the energy consumption of auxiliary components such as pumps and blowers. To take into account the power consumption of the entire electrolyser system, the system efficiency can be defined as:

$$\eta_{sys} = \frac{\dot{V}_{H_2} \bullet HHV_{H2}}{P_{module} + P_{blower} + P_{pumps}} \tag{11}$$

As illustrated by equation (11), the module efficiency significantly influences the system efficiency, as a more efficient module consumes less power, leading to higher overall system efficiency. Following the module, the blower exhibits the highest power consumption in the AEL system. Therefore, implementing a more efficient cooling system with lower power consumption in the blower may substantially enhance the efficiency of the AEL system.

### 2.2.2. Ammonia synthesis

As illustrated in Fig. 2, the production of green ammonia relies on the utilization of a ruthenium-based catalyst for synthesizing ammonia and the implementation of sorbent layers for absorption and separation of the synthesized ammonia from unreacted gases. In this case, the rate of ammonia generation over the 5 %Ru/10 %Cs/$CeO_2$ catalyst can be described using the following equation [28]:

$$r = 2.9\exp\left(\frac{-62139}{RT}\right)P_{N_2} - 2.31 \times 10^9 \exp\left(\frac{-133714}{RT}\right){P_{NH_3}}^{1.3}{P_{H_2}}^{-2.5} \tag{12}$$

where r denotes the rate of ammonia production in $\frac{mol_{NH_3}}{g_{cat} min}$, while $P_{N_2}$, $P_{H_2}$, and $P_{NH_3}$ represents the partial pressure of nitrogen, hydrogen and ammonia in bar, respectively. In this study, the reactors employed to produce ammonia over ruthenium-based catalysts were simulated using plug flow reactor models accessible in Aspen Plus. Accordingly, the Langmuir-Hinshelwood-Hougen-Watson (LHHW) kinetic formulation was utilized to simulate the ammonia synthesis reaction, employing the rate expression provided by Equation (12) [37].

As mentioned before, this study employs $MgCl_2$ for ammonia absorption and separation, aiming to surpass equilibrium limitations and convert over 90 % of the fed hydrogen into ammonia. The rate of ammonia adsorption utilizing $MgCl_2$ as the sorbent material is provided as follows [26]:

$$r_{abs} = \begin{cases} \dfrac{k_a\left(P_{NH_3} - P_{eq}\right)^7}{K + \left(P_{NH_3} - P_{eq}\right)^6} & if\ P_{NH3} > P_{eq}\ \&\ q_{NH3} < q_{NH3}^{max} \\ 0 \quad if\ P_{NH3} < P_{eq}\ or\ q_{NH3} = q_{NH3}^{max} \end{cases} \tag{13}$$

where $q_{NH3}^{max}$ is the maximum capacity of the sorbent material which can be considered 4.2 $mol_{NH_3}/kg_{MgCl_2}$, while $k_a$ and K are constants and given in reference [26], $P_{NH_3}$ is the partial pressure of ammonia in bar and $P_{eq}$ represents the equilibrium pressure which can be calculated using the following equation:

$$P_{eq} = \exp\left(\frac{\Delta H_{abs}}{R}\left(\frac{1}{T} - \frac{1}{T_{ref}}\right)\right) \tag{14}$$

where $\Delta H_{abs}$ represents the heat of absorption, with a value of −87,000 J/mol, while T stands for the temperature of the sorption bed, and $T_{ref}$ denotes the reference temperature, set at 648.05 K. According to Equation (13), the sorbent material can absorb and separate ammonia from the gas mixture when the partial pressure of ammonia exceeds the equilibrium pressure, and the sorbent material has not reached its maximum capacity. Otherwise, the sorbent material will be unable to absorb ammonia. In this study, a one-dimensional transient model was developed to generate breakthrough curves and assess pressure drops within the sorbent beds. In this model, it was assumed that the sorbent material exhibits 100 % selectivity towards ammonia, with zero absorption rates for hydrogen and nitrogen. The same assumption was made in reference [26], since $MgCl_2$ is known as an ammonia-selective absorbent due to its exceptionally high selectivity toward ammonia [38,39]. It is important to acknowledge that the supported sorbent material employed for ammonia absorption and separation might experience mass loss due to the evaporation of molten $MgCl_2$ at exceedingly high temperatures, reaching up to 800 °C, with a maximum loss of 5 %[40]. Consequently, this study disregards the mass loss of the sorbent material since it is not subjected to very high temperatures; the maximum temperature it reaches is 411 °C. This is mostly due to the separation of the sorbent material and the catalyst into different containers, ensuring that the sorbent material does not reach the very high temperatures (up to 600 °C) required for catalyst reduction. The model can calculate the molar flow rate of ammonia leaving the sorption layers during the one-hour operational period until the sorbent becomes saturated, exhibiting the breakpoint. The required mass of sorbent material can be calculated using the following equation:

$$m_{sorbent} = \frac{\dot{n}_{NH_3} \times t}{C} \tag{15}$$

where $\dot{n}_{NH_3}$ represents the ammonia productivity in each catalyst layer in mol/hr, while t and C denote the operating time (1 hour of ammonia absorption) and the capacity of the sorbent material (4.2 $mol_{NH_3}/kg_{MgCl_2}$), respectively. In this case, the calculated mass of sorbent material obtained using Equation (15) was employed in the transient model. As demonstrated later, the molar flow rate of ammonia at the outlet of sorption layers changes slightly over time until saturation of the sorbent material occurs, leading to breakthrough. Thus, disregarding the negligible variation in $NH_3$ molar flow rate, the sorbent beds can be modeled using a separator block accessible in Aspen Plus.

Once the sorption beds are saturated, they need to be regenerated through the desorption of ammonia. The desorption rate can be calculated using the following equation [26]:

$$r_{des} = \begin{cases} k_{des}(P_{eq} - P_{NH3}) & if\ P_{NH3} < P_{eq} \& q_{NH3} > 0 \\ 0 & if\ P_{NH3} > P_{eq}\ or\ q_{NH3} = 0 \end{cases} \quad (16)$$

where $k_{des}$ is a constant which is given in the reference [26]. According to Equation (15), the desorption rate is contingent upon the partial pressure of ammonia and the equilibrium pressure. Referring to Equation (14), it is evident that equilibrium pressure increases with temperature. Therefore, desorption transpires more rapidly at lower pressures and higher temperatures. In this study, a 1D transient model was likewise developed to simulate the desorption process in MATLAB.

Degradation of the sorbent materials' capacity is an important factor when using these materials for ammonia absorption and separation to exceed the equilibrium limitations in a single pass. However, it has been demonstrated that supported $MgCl_2$ is stable and history-independent, effectively maintaining its absorption capacity even after 40 cycles of absorption–desorption [41]. Therefore, this study did not take into account the deterioration of the sorbent material's capacity for ammonia absorption over multiple absorption–desorption cycles.

In this study, the Ergun equation was used to calculate the pressure drops in both catalyst beds as well as the sorption bed, as follows:

$$\Delta P = \frac{150\mu L(1-\varepsilon)^2}{d_p^2\varepsilon^3}v_s + \frac{1.75L\rho(1-\varepsilon)}{d_p\varepsilon^3}v_s^2 \quad (17)$$

where μ, L, ε, $d_p$, $v_s$, and ρ represent the dynamic viscosity of the gas mixture, the length of the bed, the bed void fraction, particle diameter, superficial velocity, and the density of the flow. respectively. In this case, the dynamic viscosity of the gaseous mixture can be calculated using the following equation [42]:

$$\mu_{mix} = \sum_i \frac{x_i\mu_i}{x_i + \sum_{j\neq i}(x_j\varphi_{ij})} \quad (18)$$

where $x_i$ and $\mu_i$ (for i = $N_2$, $H_2$, $NH_3$) denote the mole fraction and dynamic viscosity of the $i^{th}$ component, respectively. In this case, the coefficient $\varphi_{ij}$ can be calculated for each pair of components as follows:

$$\varphi_{ij} = \frac{[1 + (\frac{\mu_i}{\mu_j})^{0.5}(\frac{M_i}{M_j})^{0.25}]^2}{2\sqrt{2}(1+\frac{M_i}{M_j})^{0.5}} \quad (19)$$

where M is the molar mass of each component.

## 3. Results and discussion

This section discusses the results obtained for modeling the AEL and green ammonia production, as shown in Figs. 1 and 2. Furthermore, this section provides economic analysis, which not only estimates the cost of green ammonia production using the configuration shown in Fig. 2 but also compares the annual electricity costs of the process with the green Haber-Bosch process.

### 3.1. Performance of AEL

The variation of Faraday efficiency against current density across temperatures (ranging from 65 °C to 95 °C) is shown in Fig. 3. The temperature of the stack and the density of current flowing through the cell are the two parameters that primarily influence Faraday efficiency. Specifically, lower current densities and higher temperatures in the stack lead to a reduction in the electrical resistance of the electrolyte, resulting in a higher share of parasitic current losses along the gas pipelines and consequently, a decrease in Faraday efficiency [31,43]. It is noteworthy that the model used for Faraday efficiency appeared to offer a more accurate representation of experimental data for current density values exceeding 1500 A/$m^2$[19].

Fig. 4 illustrates the variation of required voltage and power for stacks within the module across a broad range of current densities and temperatures. It is evident that both required voltage and power

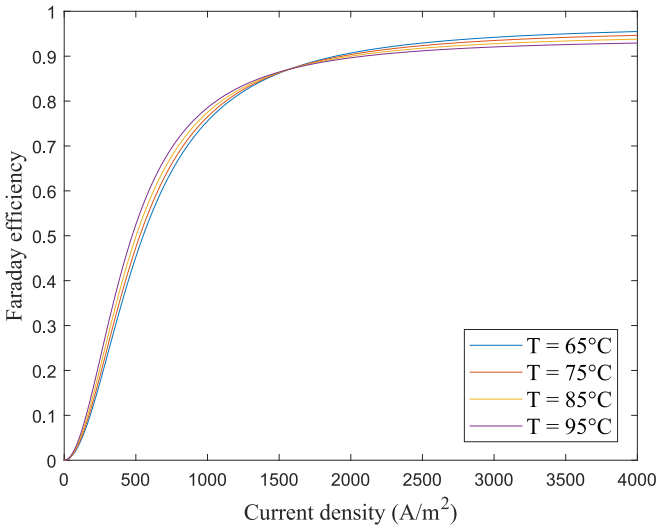


**Fig. 3.** Variation of faraday efficiency against current density for different temperatures.

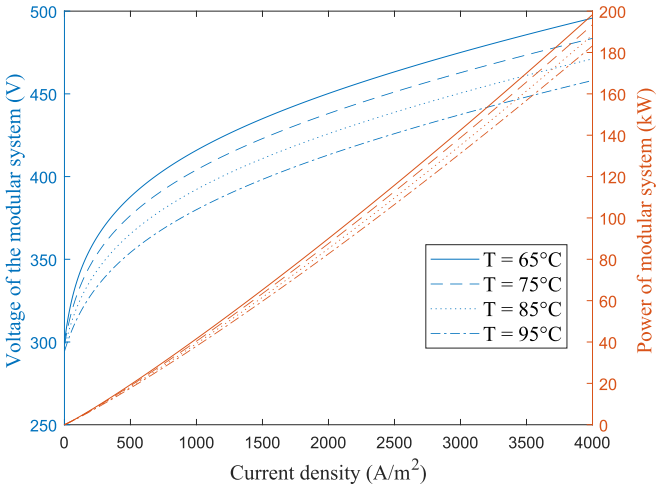


**Fig. 4.** The voltage and power of stack alkaline electrolyser.

increase with higher current densities. However, within the module, voltage and power consumption decrease with rising temperature. Consequently, operating stacks at higher temperatures may yield higher efficiencies by lowering reversible and cell voltages, thus reducing required power. Moreover, reduced cell voltage leads to decreased heat release and lower power consumption for electrolyte cooling, as discussed later.

As shown in Fig. 5, the efficiency of the module, comprising 20 stacks, increases sharply with current density. However, after reaching a maximum stack efficiency, it slightly decreases with further increases in current density. In this study, an operating current density of 2000 A/$m^2$ was selected to attain maximum efficiency for the stacks within the module. Additionally, as previously discussed, the efficiency of the modular system increases with stack temperature. Increasing the temperature leads to a progressive reduction in the voltage per cell, owing to the decreased energy requirement for electrolysis. This is mostly because of enhanced reaction kinetics and the elevated electrolytic conductivity at high temperatures [19]. In fact, despite a slight decrease in Faraday efficiency and thus the amount of generated hydrogen with increasing stack temperature, the decrease in power consumption within the stacks is more pronounced. Therefore, according to Equation (10), the module with 20 stacks demonstrates higher efficiencies at elevated

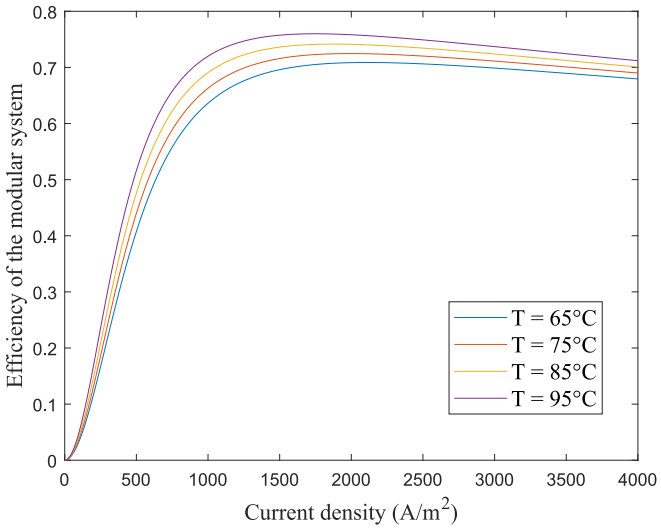


**Fig. 5.** Variation of stack efficiency against current density for different temperatures.

temperatures. Although operating stacks at higher temperatures can result in lower power consumption and increased energy efficiency, it is necessary to take into account limitations associated with the resistance of the materials composing the stack [19,33]. For this reason, a temperature of 75 °C was selected for the stacks within the module in this study.

Similarly, Fig. 6 illustrates the HTO and the purity of the generated oxygen in the AEL system. As discussed in Fig. 1, the generated oxygen undergoes purification by separating its water content using a flash. Therefore, the purity of the oxygen is influenced by both the HTO and the vapor pressure of water. According to Fig. 6, the HTO decreases as the current density increases. As mentioned earlier, the HTO, which is determined by the current density and stack temperature and pressure, not only impacts the purity of the generated oxygen but may also lead to safety concerns if it exceeds 4 % [35]. As shown in Fig. 6, the HTO increases with the rise in the stacks' temperature. Therefore, as depicted in Fig. 6, the generated oxygen exhibits higher purities at higher current densities due to lower HTO. Additionally, the purity of the generated oxygen decreases as the stacks' operating temperature increases, as it intensifies the HTO. However, as shown in Fig. 6, the HTO does not exceed 2 % even under the most unfavorable operating conditions, ensuring the safety of the hydrogen production system.

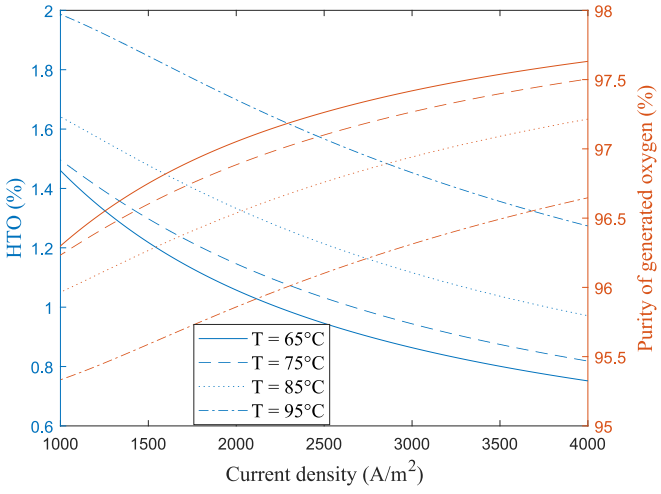


**Fig. 6.** HTO of the electrolyser stack against the current density for different temperatures.

As previously mentioned, this study utilizes a cooling tower where water, responsible for cooling the electrolyte, cools upon direct contact with air. This method proves significantly more energy efficient than cooling water using a heat exchanger, not only due to eliminating the minimum temperature approach in the heat exchanger, but also because of water cooling through evaporation. As shown in Fig. 7, the parasitic power consumption for cooling the electrolyte decreases significantly when direct water cooling is applied. It is noteworthy that power consumption in both cooling systems decreases as stack temperature increases. This means, operating the stacks at higher temperatures necessitates pressurizing a lower mass flow rate of air using the blower to cool the water and consequently the electrolyte. However, it is observed that the rate of hydrogen production using the AEL stacks decreases slightly by over 2 % as the stack temperature increases from 65 °C to 95 °C. This slight decrease is attributed to reduced Faraday efficiency, leading to a small reduction in hydrogen production, as shown in Equation (8).

Even though direct water cooling is more energy-efficient, it consumes water through evaporation. Fig. 8 shows that water evaporation within the cooling tower increases when operating the stacks at lower temperatures. At lower operating temperatures, more air is required to be introduced into the cooling tower to cool the water through direct contact. It is not only due to the lower temperatures required for cooling the electrolyte, but also the higher heat release within the stacks that necessitates removal by the water. As a consequence, the increased water loss through evaporation must be made up before the electrolyte can be cooled effectively.

Fig. 9 illustrates the variation in system efficiency when considering direct water cooling and indirect water cooling for different stack temperatures while operating the AEL system at a current density of 2000 A/m2, comparing them with the efficiency of stacks operating within the module. The system efficiency exhibits lower values than the stacks' efficiency due to the inclusion of power consumption by the pumps and the blower used in system. In other words, the efficiency of the stacks within the module, calculated using Equation (10), focuses solely on the water-splitting reaction occurring in the stacks. As a result, it only considers the power consumption within the stacks. In contrast, the system efficiency, calculated using Equation (11), accounts for the power consumption of the electrolyzer stacks, pumps, and the cooling system, which is responsible for cooling the electrolyte through either direct or indirect water-cooling processes. Consequently, the power consumption within the stacks is always lower than that of the entire system, regardless of the cooling method used, leading to higher

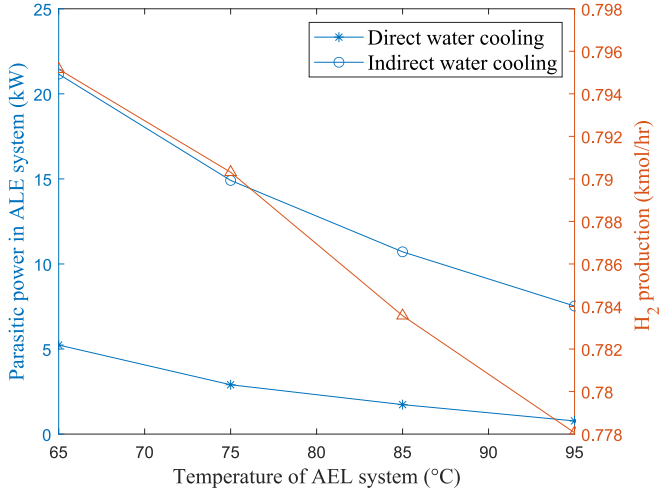


**Fig. 7.** Power consumption of auxiliary components and hydrogen production capacity of the alkaline electrolyser for different temperatures using direct and indirect cooling.

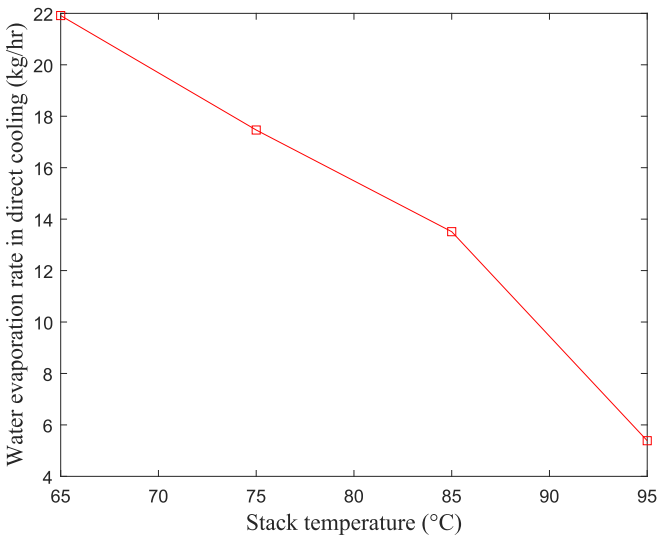


**Fig. 8.** Rate of water evaporation for cooling the alkaline electrolyser stack using direct cooling method.

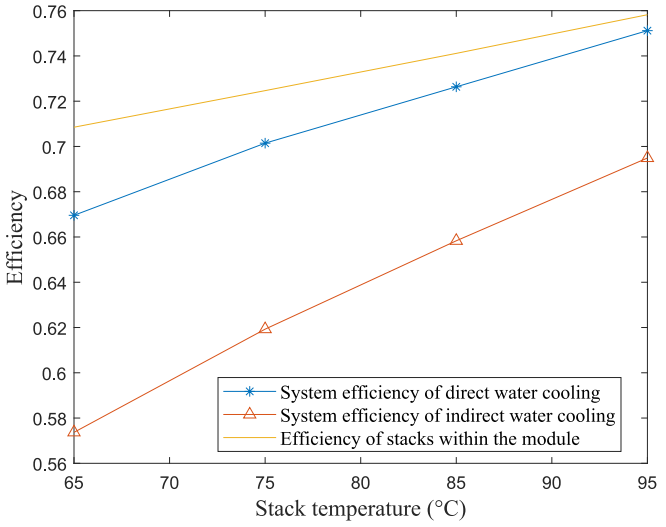


**Fig. 9.** Comparison of the system efficiency of the alkaline electrolyser using direct and indirect cooling methods with the stack efficiency.

efficiency for the stacks. Hence, Fig. 9 highlights how the system efficiency deviates from the stack efficiency primarily due to the use of a cooling system. According to Fig. 9, this deviation is noticeably lower when using the direct cooling system. Nevertheless, both the stacks' efficiency and the system efficiency increase as the temperature of the stacks rises. Notably, the system efficiency of the AEL demonstrates a steeper increase compared to the stacks' efficiency, primarily attributed to decreased power consumption in both the stacks and the cooling system with increasing temperature. Additionally, the figure highlights how the direct cooling system can enhance the efficiency of the AEL system. Direct water cooling, as depicted in Fig. 9, yields a system efficiency substantially closer to the stacks' efficiency than the indirect cooling system. For instance, according to this figure, the direct water-cooling system can enhance the system efficiency by 13.27 % when operating the system at 75 °C.

### 3.2. *Performance of the proposed green ammonia production process*

To validate the obtained model results, the synthesis of ammonia inside the reactor was simulated under the same conditions as those previously described in reference [28]. These results showed a good fitting between the model predictions and the experimental data as shown in Fig. 10.

The variation in reaction rate for ammonia synthesis across the length of the reactor, specifically at the first, seventh, and 15th catalyst beds was analyzed, and the results are shown in the Fig. 11. To optimize the conversion, the inlet temperature to the catalyst layers is progressively lowered from the first to the last catalyst bed. Despite the decrease in temperature, combined with pressure drops leading to reduced reaction rates as shown in Fig. 11, it effectively enhances conversion by delaying the achievement of equilibrium in catalyst beds. In fact, ammonia conversion and separation lead to a decrease in flow rate and GHSV as one progresses from the initial to the final catalyst layer. This trend triggers an increase in the reaction rate and hastens reaching the equilibrium, resulting in lower conversion. Hence, it is crucial to adjust the inlet temperature of reactants entering the catalyst layers to prevent early equilibrium and fully utilize the potential of each catalyst layer for ammonia conversion. This optimization enhances the overall conversion efficiency achieved in a single pass through the reactors.

Ammonia production rate and the mole fraction of synthesized ammonia at the outlet of the catalyst layers are displayed at Fig. 12. Noticeably, there is a decline in the ammonia production rate as we progress from the first to the last catalyst layers. This decrease can be associated primarily to the reduction in the flow rates of reactants entering the catalyst layers. Conversely, the mole fraction of synthesized ammonia increases from the first to the last catalyst layer. This rise is mainly due to the decrease in flow rate and GHSV of the reactants entering the catalyst layers. Consequently, the first catalyst bed yields the highest amount of ammonia with the lowest partial pressure, whereas the last catalyst layer yields the lowest amount of ammonia with the highest partial pressure.

The increase of the partial pressure of ammonia from the first to the last catalyst layer directly influences the absorption and separation of ammonia. Considering Equation (13), the rate of ammonia absorption depends on the partial pressure of ammonia, resulting in an increase in ammonia absorption rate from the first to the last sorption layer. Furthermore, the decrease in molar flow rates of nitrogen and hydrogen entering the sorption layers due to ammonia conversion as progeressing from the first to the last sorption layer results in the absorption of more ammonia to attain the equilibrium pressure. As shown by the breakthrough curves depicted in Fig. 13, the molar flow rate of ammonia at the outlet of the last sorption layer is lower. Furthermore, as previously mentioned, the flow rate of ammonia at the outlet of the sorbent layers

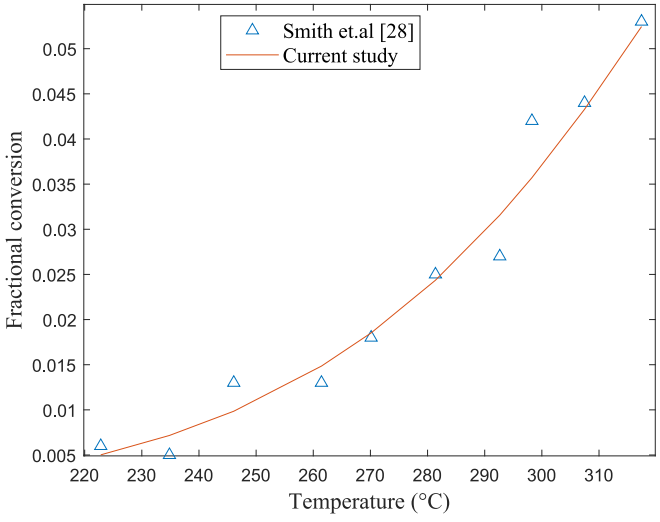


**Fig. 10.** Validation of the model for ammonia synthesis against experimental data.

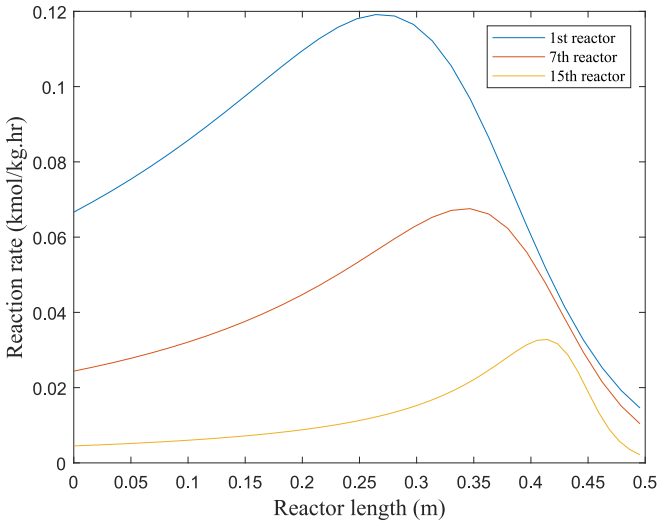


**Fig. 11.** Reaction rates of ammonia synthesis in the first, seventh, fifteenth catalyst beds.

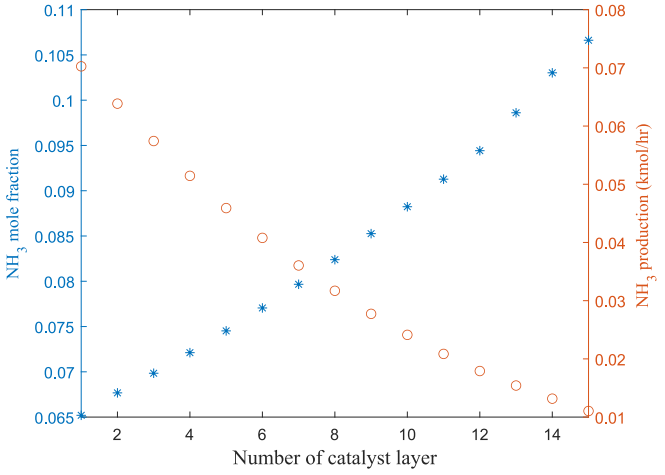


**Fig. 12.** $NH_3$ mole fraction and $NH_3$ production rate the outlet stream of different catalyst beds.

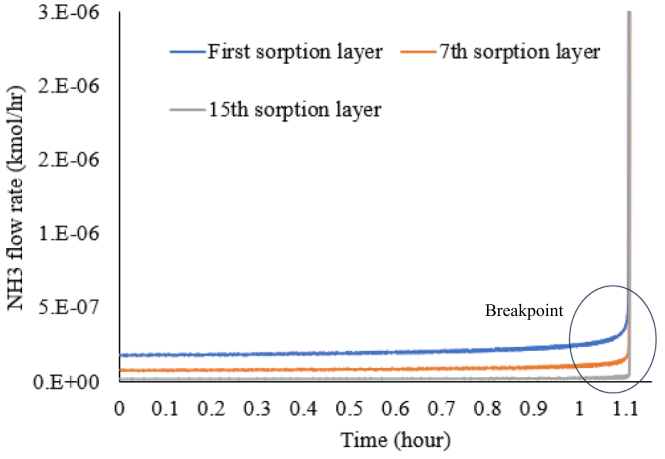


**Fig. 13.** Breakthrough curves for the first, seventh, and the last sorption beds against the time.

remains relatively stable until saturation, facilitating their modeling in Aspen Plus using a separator block. However, upon saturation of the sorbent layers, there is a sharp increase in the molar flow rate of ammonia.

It is noteworthy that the pressure drop within the sorption beds increases over time. Thus, as illustrated in Fig. 14, the outlet pressure gradually decreases from the first sorption layer. Initially, during the sorption process, ammonia is absorbed and removed by the sorbent material positioned at the beginning of the sorption layer. Consequently, the gas flow rate and velocity passing through the sorption layer decrease, resulting in lower pressure drops according to equation (17). However, as ammonia is absorbed and the sorbent material becomes saturated, a higher flow passes through the bed, leading to increased pressure drops. Therefore, the average outlet pressure from the sorbent layers was considered for modeling them in Aspen Plus using the separator.

Fig. 15 discusses the regeneration of the sorbent material once it becomes fully saturated after one hour of operation. According to equation (16), the rate of ammonia desorption is closely linked to both the equilibrium pressure and the partial pressure of ammonia. Consequently, the sorbent material can be regenerated more rapidly at lower pressures and higher temperatures, as the equilibrium pressure increases with temperature. In this study, the regeneration process occurs at a pressure of 2 bars and a temperature of 411 °C. As depicted in Fig. 15, the sorbent material can be fully regenerated in 30 min under these conditions. While lower pressures could be utilized to regenerate the sorbent material at lower temperatures, a pressure of 2 bars was selected to prevent the sweep flow of $N_2$ and to achieve ammonia with higher purities. In this scenario, the pressure gradient (i.e., 2 bars in the sorption container and atmospheric pressure at the outlet of the container) facilitates the discharge of desorbed ammonia without requiring sweep flow. Therefore, to regenerate the sorbent material, the pressure within the sorbent container is reduced to 2 bars, followed by heating to 411 °C. As can be seen, the flow rate of ammonia at the outlet of the container is initially high during the desorption process, gradually decreasing as the partial pressure of ammonia within the container increases. Ultimately, it diminishes to zero once the sorption material is completely regenerated. Assuming the dead volume of the container is entirely filled with $N_2$ and $H_2$, which are uniformly discharged during the desorption period, ammonia can be desorbed with 99.7 % purity.

This study also assesses the performance of the green Haber-Bosch process in comparison to the proposed configuration depicted in Fig. 2. The evaluated green Haber-Bosch process is illustrated in Fig. 16. Notably, this study employs the same catalyst for the green Haber-Bosch

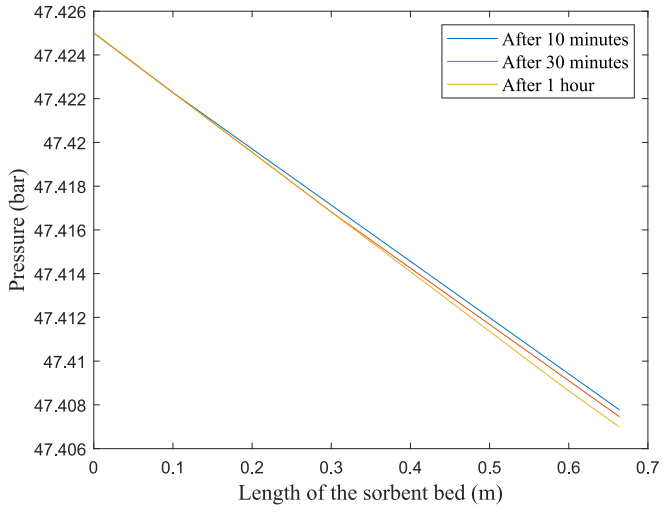


**Fig. 14.** Variation of the pressure output from the first sorbent bed with the operation time.

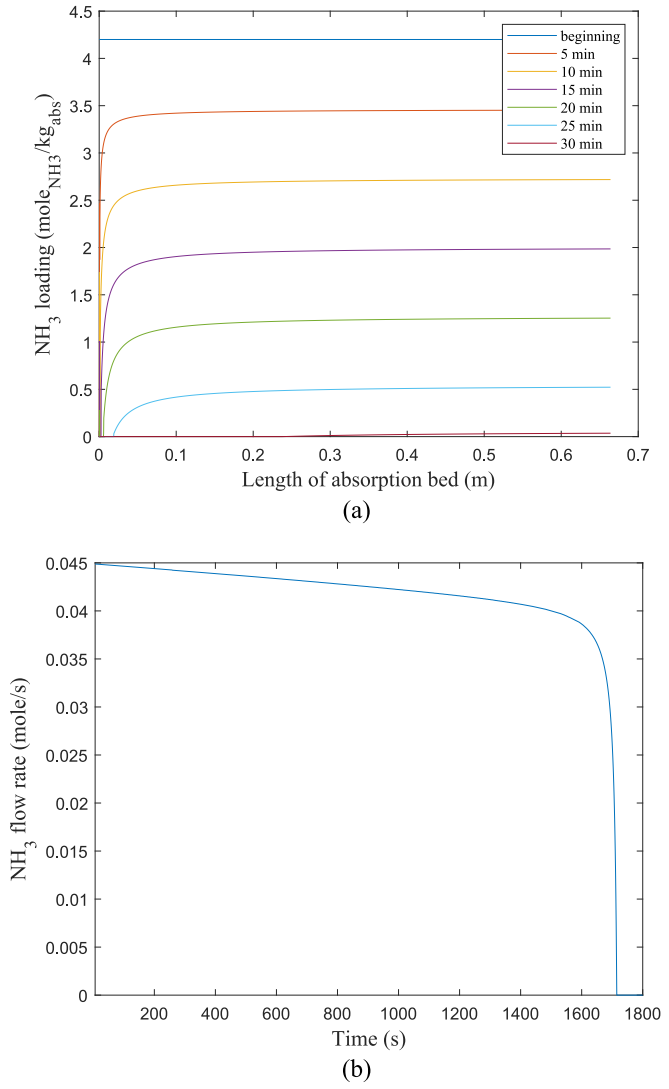


**Fig. 15.** (a) Variation of (a) $NH_3$ loading with the time in the first sorption bed (b) NH3 flow rate at the outlet of the first absorption layer during the regeneration process.

process, consisting of two reactors operating in adiabatic mode, with an intercooler cooling the gas mixture (state 6) down to 400 °C. The Haber Bosch process under consideration operates at a pressure of 160 bars with an inlet temperature of 450 °C (state 5). This process employs a water-cooled chiller with a coefficient of performance (COP) of 3.2 to condense ammonia at −20 °C and separate it from the unreacted gases (state 12). Table 2 indicates the characteristics of streams shown in Fig. 16. It is worth noting that the trace amount of argon (Ar) in the nitrogen stream (state 1) is due to impurities in the nitrogen supplied by CASU.

Fig. 17 compares the power consumption of the process depicted in Fig. 2 with that of green Haber Bosch process. As illustrated, the green ammonia process not only saves power by eliminating the need for a chiller for ammonia condensation and purification but also consumes significantly less power for pressurizing the reactants. Consequently, the power consumption of the proposed process is 46.2 % lower than that of the green Haber-Bosch process. It is worth noting that this study assumes complete heat recovery during the regeneration of sorbent material, achieved by cooling the regenerated bed to heat up the fully saturated one.

Hydrogen storage plays a critical role in green ammonia production. It not only guarantees continuous ammonia production using intermittent renewable energy sources but also contributes to more efficient use of renewable electricity. In this case, when renewable energy is plentiful, excess hydrogen can be produced and stored at low electricity costs, allowing for continuous ammonia production even when renewable energy sources are unavailable. To evaluate the impacts of hydrogen storage on the performance of green ammonia production and highlight its economic advantages, developing transient models is of paramount importance. Although this study has developed steady-state models for green ammonia production, some advantages of hydrogen storage can still be investigated. Continuous operation of the green ammonia production process, enabled by hydrogen storage, avoids shutdowns due to renewable power outages and consequently prevents heat losses in the process. When the green ammonia production process is shut down due to renewable power outages, it is necessary to reheat the catalyst and saturated sorbent materials. In this scenario, a large amount of heat (105.519 MJ) must be supplied to the process after each shutdown, which can be avoided by continuous operation using hydrogen storage.

### 3.3. Economic analysis

This study evaluates the initial investment costs and operating expenses associated with the green ammonia production process discussed herein. The initial investment costs for components, shown in Figs. 1 and 2, were estimated using Aspen Process Economic Analyzer (APEA) and are given in Table 3, while the operating costs are calculated based on the electricity spot price in Denmark, available in reference [44]. It is worth noting that the APEA utilizes data from the flowsheet to size the components and accurately estimate their weight both before and after installation by considering their size and selected materials. Consequently, it provides precise cost estimates for the components after installation. Additionally, the green ammonia production facility depicted in Figs. 1 and 2 does not run continuously all year round as it

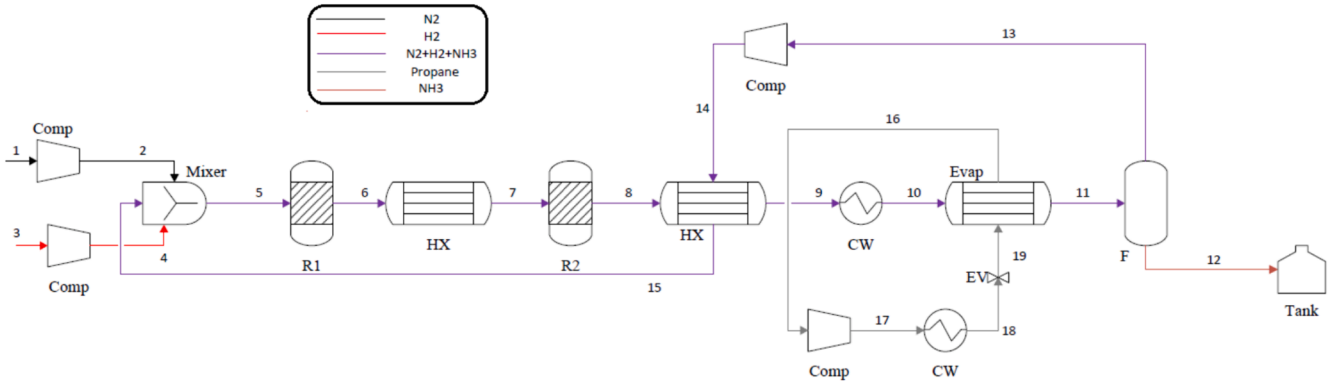


**Fig. 16.** Green Haber-Bosch process for ammonia production (Evap: Evaporator).

**Table 2**
Characteristics of streams of green Haber-Bosch process shown in Fig. 16.

| Stream number in Fig. 1 | Temperature (°C) | Pressure (bar) | Mass flow (kg/hr) | Composition (mol%) | | | | |
|---|---|---|---|---|---|---|---|---|
| | | | | $N_2$ | $H_2$ | $NH_3$ | Ar | Propane |
| 1 | 13 | 1 | 7.39378 | 0.999743 | 0 | 0 | 0.0002566 | 0 |
| 2 | 450 | 160.3 | 7.39378 | 0.999743 | 0 | 0 | 0.0002566 | 0 |
| 3 | 17 | 6.4 | 1.596 | 0 | 1 | 0 | 0 | 0 |
| 4 | 450 | 160.3 | 1. 596 | 0 | 1 | 0 | 0 | 0 |
| 5 | 450 | 160 | 26.389147 | 0.235402 | 0.750052 | 0.0139085 | 0.000637 | 0 |
| 6 | 646.613 | 159.999 | 26.389147 | 0.2030154181 | 0.658257894 | 0.1380115247 | 0.0007151 | 0 |
| 7 | 400 | 159.699 | 26.389147 | 0.2030154181 | 0.658257894 | 0.1380115247 | 0.0007151 | 0 |
| 8 | 507.135 | 159.699 | 26.389147 | 0.1824685964 | 0.600022127 | 0.2167446354 | 0.0007646 | 0 |
| 9 | 174.9219294 | 159.399 | 26.389147 | 0.1824685964 | 0.600022127 | 0.2167446354 | 0.0007646 | 0 |
| 10 | 17 | 159.099 | 26.389147 | 0.1824685964 | 0.600022127 | 0.2167446354 | 0.0007646 | 0 |
| 11 | −20 | 158.799 | 26.389147 | 0.1824685964 | 0.600022127 | 0.2167446354 | 0.0007646 | 0 |
| 12 | −20 | 158.799 | 8.97867708 | 0.0013413127 | 0.004026786 | 0.99443348 | 0.0001984 | 0 |
| 13 | −20 | 158.799 | 17.4010679 | 0.2280866106 | 0.750089978 | 0.0209058697 | 0.0009175 | 0 |
| 14 | −17.328 | 160.3 | 17.4010679 | 0.2280866106 | 0.750089978 | 0.0209058697 | 0.0009175 | 0 |
| 15 | 450 | 160 | 17.4010679 | 0.2280866106 | 0.750089978 | 0.0209058697 | 0.0009175 | 0 |
| 16 | 13.766 | 1.9 | 17.4 | 0 | 0 | 0 | 0 | 1 |
| 17 | 89.995 | 9 | 17.4 | 0 | 0 | 0 | 0 | 1 |
| 18 | 18 | 8.7 | 17.4 | 0 | 0 | 0 | 0 | 1 |
| 19 | –22.913 | 2.2 | 17.4 | 0 | 0 | 0 | 0 | 1 |

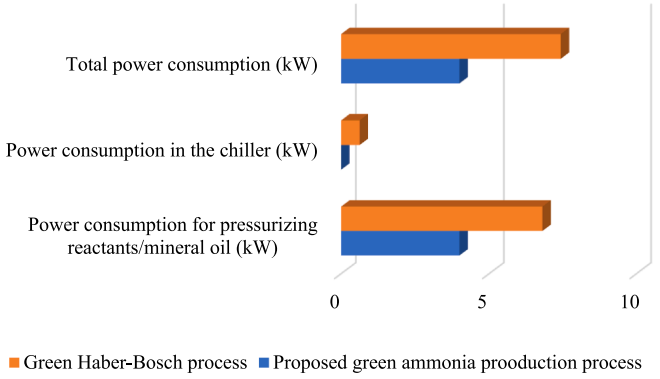


**Fig. 17.** Comparison of the power consumption of the green Haber-Bosch process (depicted in Fig. 16 with ammonia condensation) with the proposed green ammonia production process (outlined in Fig. 2 and based on ammonia absorption).

**Table 3**
Summary of initial investment costs for ammonia production plant.

| Equipment type | Costs (M€) |
|---|---|
| AEL | 0.19 |
| Catalyst and sorbent material | 0.00187 |
| Reactors and containers for sorbent material | 0.183 |
| Compressors | 0.242 |
| Pumps | 0.005 |
| Heat exchangers | 0.08 |
| Distillation columns | 0.17 |
| Flash tank | 0.015 |
| Total component costs | 0.887 |
| Costs of establishing the plant | 4.17 |

requires periodic maintenance shutdowns. Therefore, this study assumes a yearly maintenance shutdown lasting six weeks for the facility. Specifically, the primary shutdown period spans three weeks, encompassing the final week of January and the first two weeks of February. In addition to the main outages, the ammonia production facility experiences short shutdowns as necessary throughout the year. These short shutdowns usually endure for 24 hours, yet their timing remains unpredictable. Consequently, in this study, three weeks of short outages were evenly dispersed throughout the year, with the assumption that a short outage occurs every 16 days, each lasting for 24 hours. During both the primary and short outages, the ammonia production plant neither generates ammonia nor consumes power. However, according to [45] in this study, it is assumed that 2.5 % of the total initial investment costs will be allocated for maintenance, which occurs within a six-week period as described here. As previously mentioned, hydrogen production via water electrolysis necessitates the use of deionized water. This study further incorporates the cost of deionized water into the calculation of operating expenses, which does not surpass $2 per ton [46]. The cost of the ruthenium-based catalyst used in this study was estimated at 321.04 USD per kilogram according to [47]. Additionally, this study considers the costs of AEL stacks to be 2000 € per kilowatt [33]. According to reference [48], the estimated cost of one ton of $MgCl_2$ is 154 €. As illustrated in Figs. 1 and 2, alongside ammonia, the process yields a significant amount of oxygen (with a total capacity of 110.28 tons per year) of relatively high quality (99.85 % from CASU and 97.1 % from AEL). Therefore, selling the generated oxygen as a by-product in the market can generate income for the ammonia production process. Consequently, this study assumes that the generated oxygen can yield income at a rate of 1.3 USD/$kg_{O_2}$ according to [49]. It is worth mentioning that after determining the cost of the utilized components depicted in Figs. 1 and 2, one can estimate the establishment costs of the plant using a Lang factor, which has a value of 4.7 according to reference [50] for fluid processing plants.

Table 4 validates the results of the economic analysis conducted by APEA. Specifically, it compares the component costs of the CASU, and green ammonia production units obtained by APEA with those reported in the literature. In this comparison, Equation (20) was used to estimate the costs of these units at the same capacity as in this study [51].

$$C = C_{ref}\left(\frac{Cap}{Cap_{ref}}\right)^{\beta}.\alpha \tag{20}$$

where $C_{ref}$, $Cap$, and $Cap_{ref}$ represent the capital costs of the reference plant, the capacity of the unit operation suitable for this study, and the capacity of the reference unit operation, respectively. These parameters are provided in Table 4. Furthermore, β is the scaling exponent with a value of 0.5, while α is the overall installation factor, which is equal to 1.

Fig. 18 illustrates the cost of ammonia production for the years 2021, 2022, and 2023. It is evident that selling the produced oxygen as a by-product yields a substantial amount of income, significantly contributing to the reduction of ammonia production costs. Additionally, the costs of deionized water do not exert a significant impact on the overall ammonia production costs. Conversely, electricity costs and maintenance costs, largely influenced by the AEL, make the highest

**Table 4**
Comparison of capital costs of CASU and ammonia production unit with the available literature.

| Unit | Reference capacity ($Cap_{ref}$) | Capacity of unit in this study ($Cap$) | Reference cost of the unit ($C_{ref}$) | Calculated costs using APEA | Estimated cost based on the cost of reference unit using Equation (20) ($C$) | Reference |
|---|---|---|---|---|---|---|
| CASU | 18,000 $ton_{air}$/day | 308.156 $kg_{air}$/day | 54.2 M$ | 245,200 $ | 224,258 $ | [52] |
| Ammonia production | 100 $kg_{NH_3}$/hr | 8.53 $kg_{NH_3}$/hr | 2.243 M$ | 390,300$ | 371,000 $ | [20] |

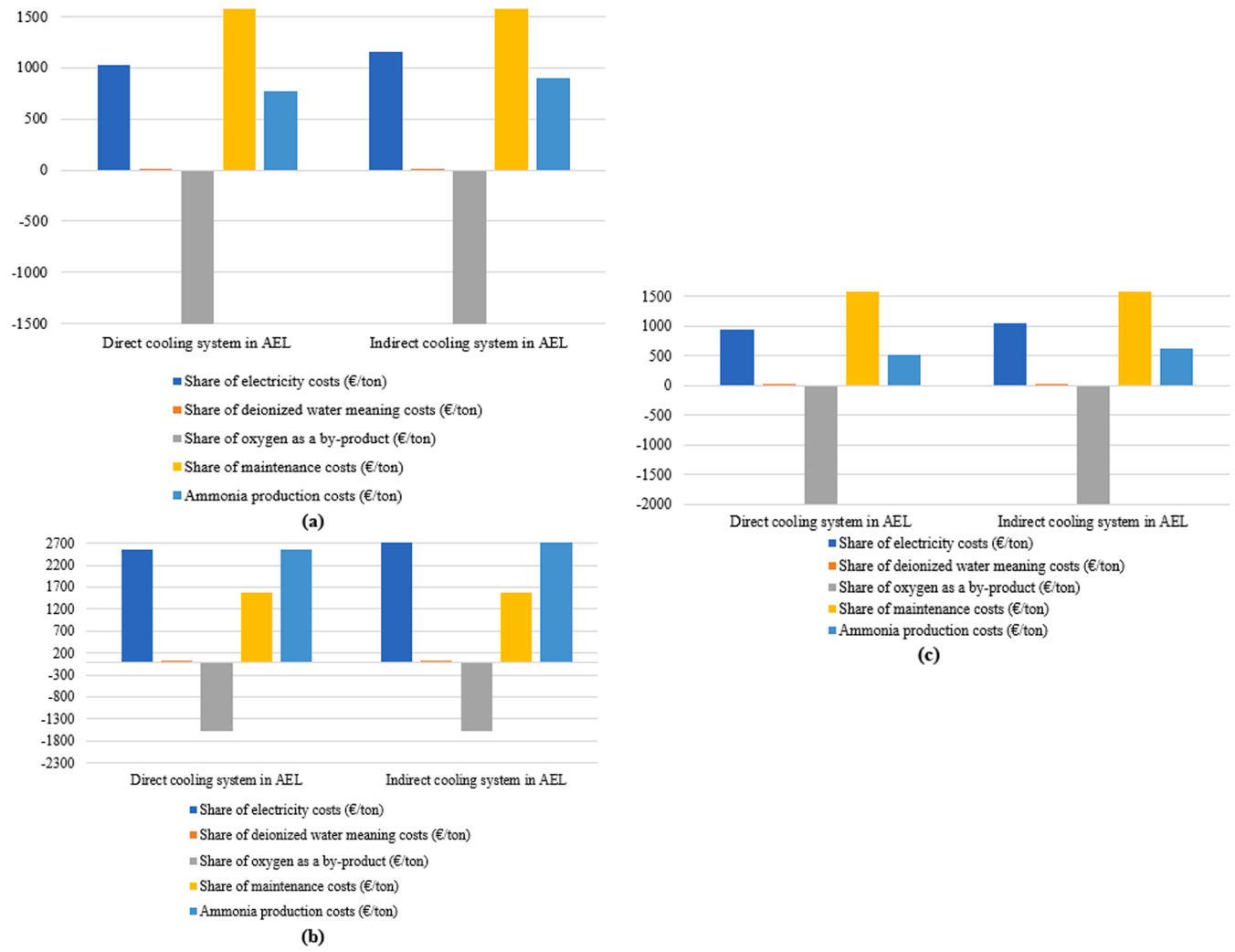


**Fig. 18.** Costs of green ammonia production in (a) 2021 (b)2022 (c)2023 when using direct and indirect cooling methods for cooling down the AEL.

contributions to the ammonia production expenses. Furthermore, the chosen cooling method for the AEL notably affects the electricity costs and, consequently, the ammonia production costs. According to Fig. 18, opting for the direct cooling method instead of the indirect method can lead to a reduction in ammonia production costs by 14.2 %, 11.1 %, and 18.44 % in 2021, 2022, and 2023, respectively.

Fig. 19 also compares the annual electricity costs of the proposed configuration for ammonia production shown in Fig. 2 with the green Haber-Bosch process discussed in Fig. 16. According to this figure, the annual electricity costs for ammonia production decrease by 3.5 % based on the electricity spot price due to power savings in the proposed process. Consequently, the figure indicates that the difference in total annual electricity costs between the green Haber-Bosch process and the process introduced in this study is not significant. The primary reason for this comparatively small difference is the inclusion of the AEL, which consumes significantly more power than the ammonia production processes.

## 4. Conclusion

This study evaluated the efficiency of a decentralized green ammonia production plant utilizing an AEL system for hydrogen production and CASU for nitrogen production. It employed a 5 %Ru/10 %Cs/$CeO_2$ catalyst to facilitate the conversion of reactants into ammonia. A modular AEL system consisting of 20 stacks was employed to provide the necessary hydrogen through water electrolysis, while a CASU supplied the required nitrogen for the ammonia synthesis reaction. The study investigated the effectiveness of cooling the electrolyte through direct water cooling in a cooling tower, comparing its efficiency with indirect cooling water in the heat exchanger. Furthermore, a novel configuration for ammonia production was proposed, capable of exceeding single-pass equilibrium by utilizing ammonia absorption and separation to convert

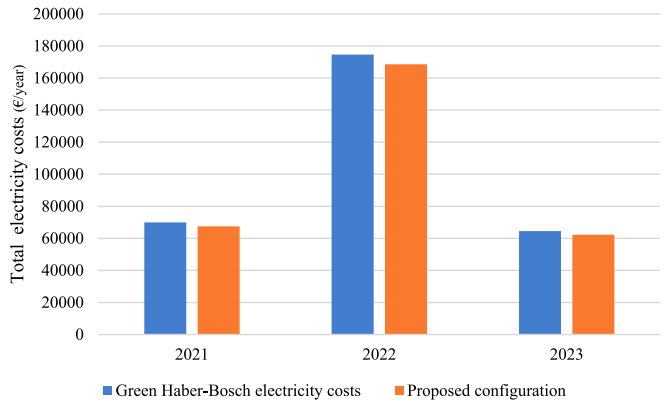


**Fig. 19.** Comparison of annual electricity costs between the green Haber-Bosch process (illustrated in Fig. 16 with ammonia condensation) and the proposed green ammonia production process (outlined in Fig. 2 based on ammonia absorption), using electricity spot prices from 2021 to 2023.

over 90 % of fed hydrogen into ammonia in a single pass. This process can synthesize ammonia at elevated temperatures and subsequently separate it using $MgCl_2$ as a sorbent material at lower temperatures. This study conducted an economic analysis on green ammonia production, calculating both initial investment costs and operating expenses. Furthermore, it compared the performance of the proposed configuration with that of the green Haber-Bosch process. While the cost of AEL is anticipated to decrease significantly in the future, leading to reduced costs in green ammonia production, its large-scale application necessitates substantial water usage, posing a critical challenge, particularly in regions struggling with drought. Consequently, it is of paramount importance to further evaluate green hydrogen production using wastewater and biogas and to utilize these methods alongside water electrolysis in the future. The following conclusions were drawn from this study:

- Direct water cooling to lower the electrolyte temperature can improve the system efficiency of the AEL by 13.27 % when operating at 75 °C and a current density of 2000 A/m$^2$.
- To achieve maximum hydrogen conversion when employing consecutive catalyst and sorption beds, it is necessary to reduce the reactants' temperature to prevent early equilibrium due to the decrease in GHSV resulting from ammonia conversion and separation, thereby utilizing the entire catalyst bed. In this scenario, the reactants' temperature was lowered from 437 °C to 300 °C upon entry into both the first and the last catalyst beds.
- The mole fraction and partial pressure of ammonia at the outlet of the catalyst layers increase progressively from the first to the last catalyst layers, thereby enhancing ammonia absorption and separation in the corresponding sorption layer. However, the rate of ammonia production decreases as one progresses from the first to the last catalyst layer.
- This study suggests that adopting the proposed ammonia production method can decrease the power consumption of green ammonia production by 46.2 % compared to the green Haber-Bosch process, resulting in an annual reduction of electricity costs by 3.5 %. This reduction is attributed to the lower power requirements for pressurizing the reactants and eliminating the need for a chiller for ammonia condensation and separation.
- The results of economic analysis indicated that utilizing the direct cooling method instead of the indirect method may result in a reduction in ammonia production costs by 14.2 %, 11.1 %, and 18.44 % in 2021, 2022, and 2023, respectively.

It is noteworthy that scaling up the process discussed in this study poses some challenges. In this scenario, it is essential to design the catalyst layers appropriately, taking into account a suitable gas hourly space velocity to achieve a relatively high ammonia production yield within each catalyst layer, thereby enabling the sorbent material to effectively absorb the generated ammonia. Moreover, the capacity of the sorbent material should be enhanced for large-scale applications. Otherwise, a large amount of sorbent material would be required, potentially leading to significant pressure drops, particularly when the diameter of the sorbent bed is small. The current study did not take into account the dynamic behavior of green ammonia production. Therefore, it is essential to develop a dynamic model for hydrogen production using the AEL and CASU, as well as for ammonia synthesis using the proposed configuration. It enables the evaluation of the positive economic impacts of hydrogen storage on green ammonia production. Utilizing hydrogen storage vessels is crucial for meeting demand and reducing power consumption during periods without renewable energy sources, ensuring continuous green ammonia production. Additionally, future studies can use the EnergyPLAN tool to evaluate green ammonia production at national levels and utilize its flexible demand option to further investigate the positive economic impacts of hydrogen storage when producing green ammonia.

## Funding

The authors acknowledge the financial support from HySTrAm project, Grant Agreement Number 101,058,643.

## CRediT authorship contribution statement

**Hossein Asgharian:** Writing – original draft, Visualization, Validation, Methodology, Formal analysis, Data curation, Conceptualization. **Valeria Pignataro:** Writing – original draft, Validation, Investigation, Formal analysis. **Florin Iov:** Writing – review & editing, Supervision. **Mads Pagh Nielsen:** Writing – review & editing, Supervision. **Vincenzo Liso:** Writing – review & editing, Supervision, Resources, Project administration, Funding acquisition.

## Declaration of competing interest

The authors declare that they have no known competing financial interests or personal relationships that could have appeared to influence the work reported in this paper.

## Data availability

Data will be made available on request.

## Appendix A. Supplementary data

Supplementary data to this article can be found online at https://doi.org/10.1016/j.enconman.2024.118764.

## References

[1] Ojelade OA, Zaman SF, Ni B-J. Green ammonia production technologies: A review of practical progress. J Environ Manage Sep. 2023;342:118348. https://doi.org/10.1016/j.jenvman.2023.118348.
[2] Kang L, Pan W, Zhang J, Wang W, Tang C. A review on ammonia blends combustion for industrial applications. Fuel Jan. 2023;332:126150. https://doi.org/10.1016/j.fuel.2022.126150.
[3] Lychnos G, Tamainot-Telto Z. Performance of hybrid refrigeration system using ammonia. Appl Therm Eng Jan. 2014;62(2):560–5. https://doi.org/10.1016/j.applthermAELng.2013.10.013.
[4] Pearson A. Refrigeration with ammonia. Int J Refrig Jun. 2008;31(4):545–51. https://doi.org/10.1016/j.ijrefrig.2007.11.011.
[5] Baumann M, BaxendAEL IR. The synthesis of active pharmaceutical ingredients (APIs) using continuous flow chemistry. Beilstein J Org Chem Jul. 2015;11:1194–219. https://doi.org/10.3762/bjoc.11.134.
[6] Tallaksen J, Bauer F, Hulteberg C, Reese M, Ahlgren S. Nitrogen fertilizers manufactured using wind power: greenhouse gas and energy balance of

community-scAEL ammonia production. J Clean Prod Nov. 2015;107:626–35. https://doi.org/10.1016/j.jclepro.2015.05.130.
[7] Leigh Krietsch B. Industrial ammonia production emits more CO2 than any other chemical-making reaction. Chemists want to change that [Online].Available: Chem Eng News 2019;97(24):1–15. https://cen.acs.org/environment/green-chemistry/Industrial-ammonia-production-emits-CO2/97/i24.
[8] Chehade G, Dincer I. Progress in green ammonia production as potential carbon-free fuel. Fuel Sep. 2021;299:120845. https://doi.org/10.1016/j.fuel.2021.120845.
[9] Zamfirescu C, Dincer I. Using ammonia as a sustainable fuel. J Power Sources Oct. 2008;185(1):459–65. https://doi.org/10.1016/j.jpowsour.2008.02.097.
[10] Tornatore C, Marchitto L, Sabia P, De Joannon M. Ammonia as Green Fuel in Internal Combustion Engines: State-of-the-Art and Future Perspectives. Front Mech Eng Jul. 2022;8. https://doi.org/10.3389/fmech.2022.944201.
[11] Bicer Y, Dincer I. Clean fuel options with hydrogen for sea transportation: A life cycle approach. Int J Hydrogen Energy Jan. 2018;43(2):1179–93. https://doi.org/10.1016/j.ijhydene.2017.10.157.
[12] Ji M, Wang J. Review and comparison of various hydrogen production methods based on costs and life cycle impact assessment indicators. Int J Hydrogen Energy Nov. 2021;46(78):38612–35. https://doi.org/10.1016/j.ijhydene.2021.09.142.
[13] Asgharian H, et al. Techno-economic analysis of blue ammonia synthesis using cryogenic CO2 capture Process-A Danish case investigation. Int J Hydrogen Energy Jun. 2024;69:608–18. https://doi.org/10.1016/j.ijhydene.2024.05.060.
[14] Vidas L, Castro R. Recent Developments on Hydrogen Production Technologies: State-of-the-Art Review with a Focus on Green-Electrolysis. Appl Sci Dec. 2021;11(23):11363. https://doi.org/10.3390/app112311363.
[15] Li Y, et al. Active pressure and flow rate control of alkaline water electrolyzer based on wind power prediction and 100% energy utilization in off-grid wind-hydrogen coupling system. Appl Energy Dec. 2022;328:120172. https://doi.org/10.1016/j.apenergy.2022.120172.
[16] Firdous A, Prakash Barala C, Mathuria P, Bhakar R. Extended power to hydrogen operations for enhanced grid flexibility in low carbon systems. Energy Convers Manag Feb. 2024;301:117982. https://doi.org/10.1016/j.enconman.2023.117982.
[17] Wang H, Zhang Q, Li X, Ma T, Sayfieva KF. Investigation into the hydrogen production performance of a novel 5-kW hybrid-system composed of a solar steam generator directly connected with conventional solid oxide electrolysis cells. Energy Convers Manag Feb. 2024;301:118023. https://doi.org/10.1016/j.enconman.2023.118023.
[18] Mazza A, Forte A, Bompard E, Cavina G, Angelini AM, Melani M. Assessment of the role of the green hydrogen as the commodity enabling a new green dialogue among the Mediterranean shores. Energy Convers Manag X May 2024:100614. https://doi.org/10.1016/j.ecmx.2024.100614.
[19] Sánchez M, Amores E, Rodríguez L, Clemente-Jul C. Semi-empirical model and experimental validation for the performance evaluation of a 15 kW alkaline water electrolyzer. Int J Hydrogen Energy Nov. 2018;43(45):20332–45. https://doi.org/10.1016/j.ijhydene.2018.09.029.
[20] Smith C, Hill AK, Torrente-Murciano L. Current and future role of Haber-Bosch ammonia in a carbon-free energy landscape. Energy Environ Sci 2020;13(2):331–44. https://doi.org/10.1039/C9EE02873K.
[21] Frattini D, Cinti G, Bidini G, Desideri U, Cioffi R, Jannelli E. A system approach in energy evaluation of different renewable energies sources integration in ammonia production plants. Renew Energy Dec. 2016;99:472–82. https://doi.org/10.1016/j.renene.2016.07.040.
[22] Lin B, Wiesner T, Malmali M. Performance of a Small-ScAEL Haber Process: A Techno-Economic Analysis. ACS Sustain Chem Eng 2020;8(41):15517–31. https://doi.org/10.1021/acssuschemeng.0c04313.
[23] Cameli F, et al. Conceptual process design and technoeconomic analysis of an e-ammonia plant: Green H2 and cryogenic air separation coupled with Haber-Bosch process. Int J Hydrogen Energy Jan. 2024;49:1416–25. https://doi.org/10.1016/j.ijhydene.2023.10.020.
[24] Nowicki DA, Agnew GD, Irvine JTS. Green ammonia production via the integration of a solid oxide electrolyser and a Haber-Bosch loop with a series of solid electrolyte oxygen pumps. Energy Convers Manag Mar. 2023;280:116816. https://doi.org/10.1016/j.enconman.2023.116816.
[25] Lin L, et al. Full-spectrum solar energy utilization for green ammonia production via solid oxide electrolysis cell coupled with Haber-Bosch process. Energy Convers Manag Jun. 2024;310:118488. https://doi.org/10.1016/j.enconman.2024.118488.
[26] Palys M, McCormick A, Cussler E, Daoutidis P. Modeling and Optimal Design of Absorbent Enhanced Ammonia Synthesis. Processes Jul. 2018;6(7):91. https://doi.org/10.3390/pr6070091.
[27] Onuoha CE, M. J. KAEL, M. Malmali, P. J. Dauenhauer, and A. V. McCormick. Improving Absorbent-Enhanced Ammonia Separation For Efficient Small-ScAEL Ammonia Synthesis. Ind Eng Chem Res Apr. 2024;63(13):5608–17. https://doi.org/10.1021/acs.iecr.3c04351.
[28] Smith C, Torrente-Murciano L. Exceeding Single-Pass Equilibrium with Integrated Absorption Separation for Ammonia Synthesis Using Renewable Energy—Redefining the Haber-Bosch Loop. Adv Energy Mater 2021;11(13):pp. https://doi.org/10.1002/aenm.202003845.
[29] Attari Moghaddam A, Krewer U. Poisoning of Ammonia Synthesis Catalyst Considering Off-Design Feed Compositions. Catalysts Oct. 2020;10(11):1225. https://doi.org/10.3390/catal10111225.
[30] Sánchez M, Amores E, Abad D, Rodríguez L, Clemente-Jul C. Aspen Plus model of an alkaline electrolysis system for hydrogen production. Int J Hydrogen Energy 2020;45(7):3916–29. https://doi.org/10.1016/j.ijhydene.2019.12.027.
[31] A. Buttler and H. Spliethoff, "Current status of water electrolysis for energy storage, grid balancing and sector coupling via power-to-gas and power-to-liquids: A review," *Renew. Sustain. Energy Rev.*, vol. 82, no. February 2017, pp. 2440–2454, 2018, doi: 10.1016/j.rser.2017.09.003.
[32] Sakas G, Ibáñez-Rioja A, Ruuskanen V, Kosonen A, Ahola J, Bergmann O. Dynamic energy and mass balance model for an industrial alkaline water electrolyzer plant process. Int J Hydrogen Energy Jan. 2022;47(7):4328–45. https://doi.org/10.1016/j.ijhydene.2021.11.126.
[33] Brauns J, Turek T. Alkaline Water Electrolysis Powered by Renewable Energy: A Review. Processes Feb. 2020;8(2):248. https://doi.org/10.3390/pr8020248.
[34] Götz M, et al. Renewable Power-to-Gas: A technological and economic review. Renew Energy Jan. 2016;85:1371–90. https://doi.org/10.1016/j.renene.2015.07.066.
[35] V. S. and K. Holtappels. Explosion Characteristics of Hydrogen-Air and Hydrogen-Oxygen Mixtures at Elevated Pressures. In: in *International Conference on Hydrogen Safety*; 2005. p. 120001.
[36] Ipsakis D, Voutetakis S, Seferlis P, Stergiopoulos F, Elmasides C. Power management strategies for a stand-alone power system using renewable energy sources and hydrogen storage. Int J Hydrogen Energy Aug. 2009;34(16):7081–95. https://doi.org/10.1016/j.ijhydene.2008.06.051.
[37] "AspenTech." USA, 2023.
[38] Kael MJ, et al. Optimizing Ammonia Separation via Reactive Absorption for Sustainable Ammonia Synthesis. ACS Appl Energy Mater Mar. 2020;3(3):2576–84. https://doi.org/10.1021/acsaem.9b02278.
[39] Himstedt HH, Huberty MS, McCormick AV, Schmidt LD, Cussler EL. Ammonia synthesis enhanced by magnesium chloride absorption. AIChE J Apr. 2015;61(4):1364–71. https://doi.org/10.1002/aic.14733.
[40] Z. Cao, N. Grimaldos Osorio, X. Cai, P. Feng, and F. Akhtar, "Carbon-reinforced MgCl2 composites with high structural stability as robust ammonia carriers for selective catalytic reduction system," *J. Environ. Chem. Eng.*, vol. 8, no. 1, p. 103584, Feb. 2020, doi: 10.1016/j.jece.2019.103584.
[41] Wagner K, et al. Column absorption for reproducible cyclic separation in small scAEL ammonia synthesis. AIChE J Jul. 2017;63(7):3058–68. https://doi.org/10.1002/aic.15685.
[42] T. A. Davidson, "A simple and accurate method for calculatlng viscosity of gaseous mixtures," *United States Dep. Inter. - Bur. Mines*, pp. 1–12, 1993.
[43] Ulleberg O. Modeling of advanced alkaline electrolyzers: a system simulation approach. Int J Hydrogen Energy Jan. 2003;28(1):21–33. https://doi.org/10.1016/S0360-3199(02)00033-2.
[44] "Energy-Charts." https://energy-charts.info/charts/price_spot_market/chart.htm?l=en&c=DK&stacking=stacked_absolute_area&interval=year&legendItems=0000100&year=2021&download-format=text%2Fcsv.
[45] R. Yukesh Kannah *et al.*, "Techno-economic assessment of various hydrogen production methods – A review," *Bioresour. Technol.*, vol. 319, p. 124175, Jan. 2021, doi: 10.1016/j.biortech.2020.124175.
[46] Hausmann JN, Schlögl R, Menezes PW, Driess M. Is direct seawater splitting economically meaningful? Energy Environ Sci 2021;14(7):3679–85. https://doi.org/10.1039/D0EE03659E.
[47] Yoshida M, Ogawa T, Imamura Y, Ishihara KN. Economies of scAEL in ammonia synthesis loops embedded with iron- and ruthenium-based catalysts. Int J Hydrogen Energy Aug. 2021;46(57):28840–54. https://doi.org/10.1016/j.ijhydene.2020.12.081.
[48] Kohler T, Biedermann T, Müller K. Experimental Study of MgCl 2 · 6 H 2 O as Thermochemical Energy Storage Material. Energy Technol Oct. 2018;6(10):1935–40. https://doi.org/10.1002/ente.201800042.
[49] Zun MT, McLellan BC. Cost Projection of Global Green Hydrogen Production Scenarios. Hydrogen 2023;4(4):932–60. https://doi.org/10.3390/hydrogen4040055.
[50] Amigun H, B., & Von Blottnitz. Capital cost prediction for biogas installations in Africa: Lang factor approach. Environ Prog Sustain Energy An Off Publ Am Inst Chem Eng 2009;28(1):134–42.
[51] Ebrahimi A, Meratizaman M, Reyhani HA, Pourali O, Amidpour M. Energetic, exergetic and economic assessment of oxygen production from two columns cryogenic air separation unit. Energy 2015;90:1298–316. https://doi.org/10.1016/j.energy.2015.06.083.
[52] Young AF, Villardi HGD, Araujo LS, Raptopoulos LSC, Dutra MS. Detailed Design and Economic Evaluation of a Cryogenic Air Separation Unit with Recent Literature Solutions. Ind Eng Chem Res Oct. 2021;60(41):14830–44. https://doi.org/10.1021/acs.iecr.1c02818.